AN ABSTRACT OF THE DISSERTATION OF

Elnaz Hassanpour Adeh for the degree of Doctor of Philosophy in Water Resources Engineering presented on September 14, 2018.

Title: Environmental Impacts of Renewable Energy (solar and wind) on Water, Food and Energy Nexus

Abstract approved:

Chad W. Higgins

Abstract

Rapid increasing of renewable energies and the knowledge about their environmental effects are very limited. As a result, the renewable energies (e.g. solar or wind energies) will play a vital role in the future because it is well accepted by environmental friendly industries. This dissertation presents the modeling, data analysis and field experiment, developed for investigation of the interactions among microclimatological factors, land characteristics and solar/wind renewable energy production systems. The research covers multi scales from high resolution farm scales (six acres' area), mid-size large wind farms and global scales. The main idea of this research is to study the environmental impacts of renewable energies which affect the water resources and therefore the water, food and energy nexus. This research studies how renewable energy can change the water use efficiency, biomass production, energy efficiency and ultimately relates it to sustainable development. Selecting the best location, crop and

climate for renewable energy is an important key component in obtaining a sustainable development.

The first part of the dissertation includes an experimental observation study on the effects of solar panel on the adjacent microclimate and vegetation. The field study setup included installations of local weather stations and soil moisture neutron probes to monitor the microclimatological and moisture variations. The monitoring was performed both between solar arrays and outside the area (control area). The data showed that (1) the soil moisture under panels are significantly higher than the control area, (2) dry biomass of grass is higher under panels and (3) the area under panels were significantly more water efficient. The investigations on the grass species under agri-voltaic panels reveals a significant increase in late season biomass (90% more biomass) and areas under PV panels were significantly more water efficient. This is accomplished by harvesting solar excess and converting it to electricity.

Secondly, an algorithm developed using the first law of thermodynamics and solar panel efficiency solved for the energy balance equation. Solar panel efficiency found as a function of microclimatological factors include radiation, temperature, relative humidity and wind speed. The validated algorithm was then applied to the global scales. The computations of efficiencies shows the most efficient geographical locations for solar panel installations based on micro-environmental factors, but also a more generalized methodology to relate potential efficiency to land cover.

The third part of the thesis assess the crop yield and water use efficiency of major crops grown in Oregon, considering three shade levels 90%, 75% and 50%. AquaCrop model was used to evaluate the potential water use efficiency in Oregon. Our results show there is no difference in yield when shade is applied but the amount of water needed for irrigation is reduced. The biomass results showed no gain or loss occurs in different shade levels but there is a difference in the amount of irrigated water.

The forth part of the dissertation relates to the interactions of the wind turbines with farm lands. A numerical framework was developed to process the wind farm LANDSAT snap shots before and after the wind turbine installations. The numerical scheme was developed using Mapping Evapotranspiration at high Resolution with

Internal Calibration (METRIC) and can calculate and analyze evapotranspiration on the agricultural field and analyze the resulted pixel-based data. From the data analyses on Fowler wind farm (located in Indiana, US) approximately 10% more evapotranspiration was seen in agricultural fields that are co-located near wind turbines (i.e. footprints) compared to places that have no wind turbine.

Environmental Impacts of Renewable Energy (solar and wind) on Water, Food and Energy Nexus

by
Elnaz Hassanpour Adeh

A THESIS
submitted to
Oregon State University

in partial fulfillment of
the requirements for the
degree of
Doctor of Philosophy

Presented September 14, 2018
Commencement June 2019

Doctor of Philosophy dissertation of Elnaz Hassanpour Adeh presented on September 14, 2018.

APPROVED:

Major Professor, representing Water Resources Engineering

Director of Water Resources Engineering

Dean of the Graduate School

I understand that my dissertation will become part of the permanent collection of Oregon State University libraries. My signature below authorizes release of my dissertation to any reader upon request.

Elnaz Hassanpour Adeh, Author

ACKNOWLEDGEMENTS

I wish to express my appreciation to Professor Chad Higgins, my research advisor and chair of the dissertation committee, for his precious support during my doctoral program and guidance in this work. I also wish to thank Professor Higgins for the knowledge and wisdom transmitted about the several aspects of academic life. It has been a magnificent pleasure to have this long relationship with such a friendly and enthusiastic teacher.

I also wish to thank the other members of my dissertation committee, Dr. Richard Cuenca, Dr. Marc Calaf, Dr. Stephen Good for the important discussions and comments related to this study. I appreciate the support from graduate council representative Dr. John sessions for assuring that the conduct of all committee meetings and actions are in compliance with policies and procedures of the Graduate Council as presented by the Graduate School.

Deepest gratitude to my Husband, Vahid, for his encouragement, sacrifice and love. I will never be able to thank him enough for accompanying me during my doctoral studies. Accomplishing this arduous task without his support would be virtually impossible. I am blessed for having such a wonderful and lovely person standing by my side during all those years. I wish I knew how to thank my two-year old son, Soren, for his immeasurable happiness with my studies. He is the most important source of energy and enthusiasm that I have. I am also thankful for the immense support and love received from my parents during my entire life. Their effort in raising and educating me, and the patience in waiting for me to complete my graduate studies are sincerely appreciated.

I am indebted to the fellow students, faculty and staff members in the Oregon State University who contributed to the conclusion of my doctoral studies. Special thanks go to Dr. Marry Santelmann for her help with the data collection and support; to Dr. Julia Jones for serving in my qualifying examination committee; to Dr. John Selker for reviewing the paper; to Jenifer Cohen for the help with academic matters since the beginning of my application process. This research work was also in part supported by the NSF and partly USDA. This financial support is gratefully acknowledged.

CONTRIBUTION OF AUTHORS

Dr. John Selker, Dr. Marc Calaf, Dr. Stephan Good were involved with reviewing and commenting on the Journal manuscripts.

Dr. Ziru liu assisted with data collection.

Dr. Mary Santelmann helped for grass classification.

TABLE OF CONTENTS

Page

TABLE OF CONTENTS (Continued)

Page

LIST OF FIGURES

Figure Page

LIST OF FIGURES (Continued)

Figure Page

LIST OF TABLES

Table Page

General Introduction

This chapter is specified to a general introduction for all manuscripts, prepared during the doctoral research program. It involves two main parts: Interactions of solar energy on surrounding environment and effects of wind turbines on increasing the wind farms evapotranspiration that are co located with agricultural lands. The solar energy research consists of three parts, experimental, global and water, food and energy nexus study.

Solar and wind renewable energies significance and growth

The high energy demands have brought up the need for at least ten terawatts of carbon-free power by the mid-century to the world (Muradov & Veziroğlu, 2008). In other words, although the energy intensities have declined, the need will increase to about two-fold by the middle of 21st century is undeniable (Rodman & Meentemeyer, 2006a). This increase in energy demands (up to about 2-3% per year) are generally due to the high population and economy growth (Lewis & Nocera, 2006a). Additionally, the rapid increasing of renewable energies attention is happening and the knowledge about their environmental effects are very limited (Armstrong et al., 2014). As a result, the renewable energies (e.g. solar or wind energies) will play a vital role in the future because it is well accepted by environmental friendly industries. Furthermore, the fuel-based sources are not less reliable from environmental point of but also will last soon. The statistical studies show that the energy demand will increase about 40% between 2009 and 2035(IEA, 2011). This increase will get contributions from hydropower, biomass and waste, and 'other' renewable energies. These sources are predicted to increase by 70%, 55% and 600%, respectively (IEA, 2011) . As an expanding source wind power has grown tremendously. An extraordinary growth of about 238 GW happened to wind power growth between 2010 and 2011. Additionally, solar photovoltaic (PV) technology demonstrated a growth rate of 74%, which was the highest rate among all energy sources in 2011(Renewables, 2012, Armstrong et al., 2016) .

Conceptual design studies for solar and wind energy production facilities

Since the demands for renewable solar and wind energies are tremendously growing, the design basics for energy production facilities (e.g., solar arrays or wind turbines) are good to be well established. There are major factors that contribute to the conceptual design of solar and wind farm. However; the one of interest in this research is the interactive feedbacks between energy production facilities and their local environment and micro climate.

First, although the power production efficiency of solar arrays is obviously, directly related to panel temperature, other microclimatological factors can affect this efficiency like wind speed or relative humidity. On the other hand, the solar arrays that are installed in farms, can locally change the soil moisture and climate patterns, hence resulting in a different food production. A similar study can be performed for wind turbines installed near agricultural farms. While the wind production doesn't directly consume water, the local changes in boundary layer may affect the evapotranspiration regime on the farm, resulting in an increase in the water use for irrigation.

Consequently, considering the local environment/climate factors may significantly, change the basic design for renewable solar and wind energy production units. The enhanced design criteria should involve best environmental based geographical locations for decision makers. This factor can be directly used in the optimization process of basic design.

I. Feedbacks between solar arrays and local environments

The interactions between solar arrays and adjacent farms are qualitatively describable. The shaded area under panels may be different compared to open areas in water-limited fields, in terms of soil moisture, food productions or even microclimatological factors like wind speed, wind direction, temperature, relative humidity, etc. On the other hand, the panels power productivities can be changed by land cover.

I.1 Effects of solar panels on adjacent farm

The first part of this dissertation concentrates on the field and data analysis investigations that can quantitatively reveal these research questions. The knowledge about surface energy fluxes change and microclimate is limited uniquely in solar panels. For solar panel studies, although this study covered a local agricultural field in North-West which is water-limited in summer , its results can be extended to same weather regime. Additionally, the validated physics-based power efficiency calculations were extended to global scales, and will be discussed later in the second manuscript. An experimental observation study on the effects of solar panel on the adjacent microclimate and vegetation was performed. The first manuscript describes the results of this field study. Additionally, the outcome database of this research has been published (Selker et al., 2017) and the paper is accepted by minor revision and it is in with editor status for POLS one journal.

The data analysis results showed that the increased water use efficiency in the shaded areas of the field left water stored in the soil column available throughout the entire observation period. Extreme heterogeneity and spatial gradients in biomass production and soil moisture were observed as a result of the heterogeneous shade pattern of the PV array. A significant increase in late season biomass was also observed for areas under the PV panels (90% more biomass). In solar experiment the soil moisture data was extensively gathered with neutron probe and the micro climate variables gathered by Decagon sensors.

I.2 Solar power efficiency in farm and global scale as a function of microclimate

The second manuscript describes a physics-based model based on first law of thermodynamics and evaluates the solar power productivity. The solar power data obtained from Pacific Power were compared and validated against calculated values

from the developed model. The validation served as a base for extending to global scales. The goal was to both obtain the best geographical locations and landcover for solar array installations in the world. This model is applied globally using bias-corrected reanalysis datasets to map solar efficiency and potential solar power production considering the temperature, wind speed, radiation and relative humidity effects. Solar power production potential then classified based on global land cover distributions. This analysis demonstrates that crop lands have the greatest median solar potential followed by grass land, permanent wetlands, mixed forest and barren. These results help decision makers to select the most appropriate land cover for future solar energy displacement. This manuscript is ready to submit to nature energy journal.

I.3 Crop Modeling

The third manuscript explains crop response to shade as a result of water use efficiency and yield. One of the limitations of experimental study under solar panels was using native grown grasses which existed under solar panels. In this manuscript AquaCrop model is used to measure the water use efficiency and yield of the most grown crops grown in Oregon. This study shows how much water will be used if we use solar panels in agricultural land. This manuscript is ready to submit to Frontiers in Nexus.

II. The indirect water use through wind turbines that are close by agricultural farms

An investigation methodology for the effects of wind turbines on the large-scale wind farm area, was developed. The modeling framework was designed to process the satellite images before and after the wind turbine installations in a certain wind farm. Based on LANDSAT images, and using the METRIC method, the evapotranspiration on the agricultural field calculated. Using assumed wind turbine footprints the changes of evapotranspiration between inside the assumed footprints and the outside these areas were statistically checked.

The uncertainties associated with the footprint areas of wind turbines was a part of this study. These areas were investigated in terms of dimensions, distance from wind turbines and their directions based on wind direction. The fourth manuscript is a case study for which the evapotranspiration increase was calculated, i.e., Fowler Ridge wind farm (located in Indiana, US). From the initial data analyses on this farm, approximately 15% more evapotranspiration was seen in agricultural fields that are located near wind turbines compared to no wind turbine farms. This manuscript is ready to submit to water resources research journal.

Remarkable agrivoltaic influence on soil moisture, micrometeorology and water-use efficiency

Elnaz Hassanpour Adeh[1], John S. Selker[1], Chad W. Higgins[1*]

[1] Department of Biological and Ecological Engineering, Oregon State University, Corvallis, USA, 97331;

[*]Corresponding author, Email: chad.higgins@oregonstate.edu, Tel: 5417372286, Fax: 5417372082

Journal: PLOS ONE

PLOS

1160 Battery Street

Koshland Building East, Suite 225

San Francisco, CA 94111

United States

Phone: +1 (415) 624-1200 | Fax: +1 (415) 546-4090

PLOS is a nonprofit 501(c)(3) corporation, #C2354500, and is based in San Francisco, California, US.

1. Chapter 1: Remarkable agrivoltaic influence on soil moisture, micrometeorology and water-use efficiency

Elnaz Hassanpour Adeh[1*], John S. Selker[1], Chad W. Higgins[1]

[1] Department of Biological and Ecological Engineering, Oregon State University, Corvallis, USA, 97331;

[*]Corresponding author, Email: hassanpe@oregonstate.edu, Tel: 5417372286, Fax: 5417372082

1.1 Abstract

Power demands are set to increase by two-fold within the current century and a high fraction of that demand should be met by carbon free sources. Among the renewable energies, solar energy is among the fastest growing; therefore, a comprehensive and accurate design methodology for solar systems and how they interact with the local environment is vital. This paper addresses the environmental effects of solar panels on an unirrigated pasture that often experiences water stress. Changes to the microclimatology, soil moisture, water usage, and biomass productivity due to the presence of solar panels were quantified. The goal of this study was to show that the impacts of these factors should be considered in designing the solar farms to take advantage of potential net gains in agricultural and power production. Microclimatological stations were placed in the Rabbit Hills agrivoltaic solar arrays, located in Oregon State campus, two years after the solar array was installed. Soil moisture was quantified using neutron probe readings. Significant differences in mean air temperature, relative humidity, wind speed, wind direction, and soil moisture were observed. Areas under PV solar panels maintained higher soil moisture throughout the period of observation. A significant increase in late season biomass was also observed for areas under the PV panels (90% more biomass), and areas under PV panels were significantly more water efficient (328% more efficient).

1.2 Keywords

Agrivoltaic, microclimatology, soil moisture, solar panels, water use.

1.3 Introduction

Global energy demand will be doubled by mid-century due to population and economic growth (Lewis & Nocera, 2006b; Rodman & Meentemeyer, 2006b). Renewable and environmental-friendly energies will play a vital role to meet this demand.

Among all renewable energies, solar power is the most abundant and available source (Rogner & others, 2012). Solar power is also becoming more affordable. The cost of solar panels has fallen by 10% per year for the past thirty years, while production has risen by 30% per year. If costs continue to be reduced based on this historic rate, solar energy will be less expensive than coal by 2020(Trancik, 2014). The impact of wide-spread solar installations is an area of increasing interest. Regional climatology may be influenced by large scale solar installations, but simulations have provided conflicting results: 3- 4 ˚C *increase* in air temperature over solar panels compared to wildlands at night (Barron-Gafford et al., 2016), 0.1- 0.2 ˚C *decrease* in air temperature, 26 ˚C *increase* in the shaded roof top temperature compared with unshaded roof top (Scherba et al., 2011), 2 ˚C air *decrease* in desert regions (Hu et al., 2016),and a 5.2 ˚C *increase* in air temperature under solar panels (Armstrong et al., 2016).

Solar installations can occupy large land areas and sometimes compete with agriculture for the land resource (Nonhebel, 2005). Agrivoltaic systems are created when solar and agricultural systems are co-located for mutual benefit. The formal introduction of agrivoltaic systems is credited to Dupraz in 2011. Land demand for energy production decreases profoundly when agrivoltaics are used (Nonhebel, 2005). Not all agricultural crops are suitable, but plants with less root density and a high net photosynthetic rate are ideal candidates (Seidlova et al., 2009). Agrivoltaic systems have been shown to increase land productivity by 60-70% (Dupraz et al., 2011a), and increase the value of energy production system by 30% (Dinesh & Pearce, 2016). Very limited experimental research was found on the impacts of a solar arrays on agricultural production. Marrou et al. (H. Marrou et al., 2013) measured soil water potential and soil water gradient (difference between uptake and drainage) in cucumber and lettuce and revealed lower soil water potential under the panels. This water potential led to an increase in harvested final fresh weight. Another experiment by Marrou et el. (Hélène Marrou et

al., 2013) found that plants cover soil faster under the shade of solar panels. An experimental study by Dupraz et al. demonstrated that summer crops benefited of solar shade more than winter crops such as pea and wheat crops (Dupraz et al., n.d.). Co-locating agave plant below solar panels increased yield per m^3 of water used in the San Bernardino County in California (Ravi et al., 2014). Non-beneficial effects have also been observed in Welch onion fields where, photovoltaics reduced the fresh and dry matter harvest weight (Kadowaki et al., 2012).

In this paper, a field study was performed to measure the effects of a six-acre agrivoltaic solar farm on the microclimatology, soil moisture and pasture production. The experimental setup included microclimatological and soil moisture measurements from May to August 2015 in Rabbit Hills agrivoltaic solar arrays, located on the Oregon State University campus. The field data for this study is accessible through Oregon State library system (Hassanpour Adeh et al., 2017).

1.4 Material and methods

The field study was performed on a six acre agrivoltaic solar farm and sheep pasture near the Oregon State University Campus (Corvallis, Oregon, US.). The PhotoVoltaic Panels (PVPs) have been arranged in east–west orientated strips, 1.65 m wide and inclined southward with a tilt angle of 18^o. PVPs have been held at 1.1 meters above ground (at lowest point) and the distance between panels is 6 meters as shown in Figure1.1) e. The whole solar array system has a capacity of 1435 kilowatts[1]. As shown in Figure 1, the data were collected from localized zones (described hereafter) including areas below solar panels and a control area outside the agrivoltaic system. The pasture below the solar panels and the control areas were in the same paddock that was actively grazed by sheep. Exclusionary plots, to eliminate grazing pressure, were maintained with fencing. The total size of the fenced areas was limited by agricultural activities. The pasture was not irrigated, and typically experiences water stress mid-summer. The soil classification for >70% of the pasture area (control and agrivoltaic system) is Woodburn Silt clay ("Web Soil Survey - Home," n.d.). The control and treatment plots were located within Woodburn Silt clay classification areas. The intent of the field

[1] http://fa.oregonstate.edu/sustainability/ground-mounted-photovoltaic-arrays

measurements was to minimize uncontrollable differences between the treatments and control (e.g. solar forcing, soil types) and minimize impact on agricultural activities. Thus, the distance between the treatment site and the control site was kept minimum. The observations within the treatment site were further divided into three sub-treatments (Figure1.2): (1) Sky Fully Open area between panels (SFO), (2) Solar Partially Open between panels (SPO) and (3) Solar Fully Covered area under panels (SFC). SFO areas are between the edges of installed PV panels and experienced full sun. Shadow length calculation also confirms no shade covers the SFO zone(Appelbaum & Bany, 1979).SPO areas are in the penumbra and experienced episodic shade. SFC areas are directly beneath the PV panels and experienced full shade. Data from these sub-treatments were compared to the data collected from the control area outside the agrivoltaic array, where each measurement was replicated.

(a)

(b)

(c)

(d)

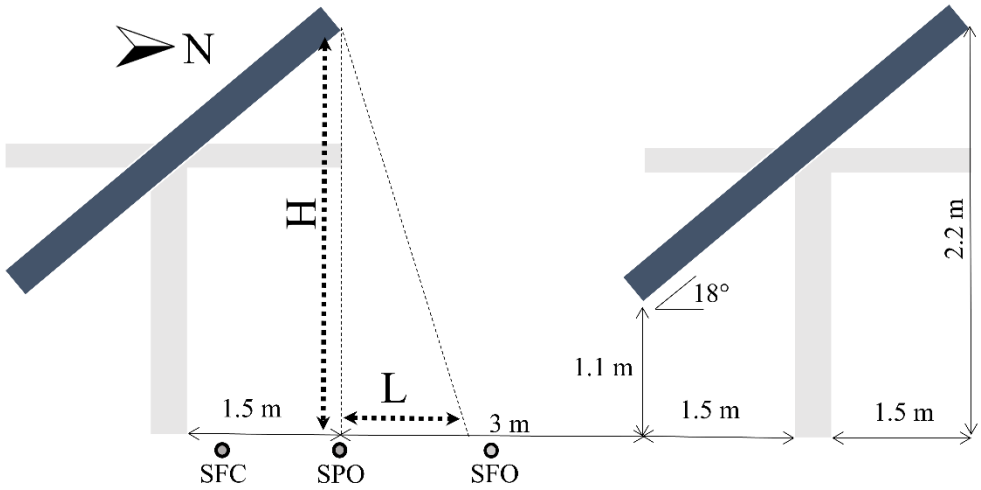

Figure1.1 a) Aerial photo of 35th Street agrivoltaic solar array, Oregon State University Corvallis campus (this photo is taken in winter and shadow pattern is different from the measurements which held in summer) Copyright: Oregon State University, b) Solar panel set up, c) Control area set up, d) Shade zones in solar panel, e) Schematic drawing of shade zones (H is object height and L is shadow length)

Shadow length (L) is calculated (Appelbaum & Bany, 1979)based on the sun latitude, solar panel height, day and time of the year the and it changes from 1.1 meters to 1.4 meters for May, June, July and August of 2015 which makes the SFO no shadow zone.Data were collected continuously in all areas from May-August 2015. Air temperature, relative humidity, wind speed and wind direction measurements were collected on 1 minute intervals. Soil moisture profiles were collected three times each week, and biomass samples were collected at the end of the observation period. Details associated with each set of measurements are explained in the following sub-sections.

Microclimatological measurements

Two atmospheric profiling stations were installed 70 meters apart: one in the control area and one near the center of the solar panel area. Micrometeorological variables were collected at four levels (0.5, 1.2, 2.0 and 2.7 m aboveground) in 1 minute intervals. The gathered variables were (1) air temperature (VP-3 Decagon Devices), (2) wind speed and directions (DS-2 Decagon Devices), (3) relative humidity (VP-3 Decagon Devices) and (4) net radiation (PYR Decagon Devices). Data were logged on EM50 data loggers (Decagon Devices). Temperature and humidity devices were calibrated in a chamber, and wind sensors were calibrated in a wind tunnel prior to installation. A Kolmogorov Smirnov test was used to detect differences in *distributions* of temperature, humidity, wind speed, wind direction, and down welling radiation between the solar array area and the control area. A two tailed t-test was used to detect differences in the *mean* temperature, humidity, wind speed, wind direction, and down welling radiation between the solar array area and the control area and standard deviation results was measured to quantify the amount of dispersion of a set of data values.

Soil moisture measurement

The soil moisture was obtained using a neutron probe device (503 DR hydro-probe Campbell Pacific Nuclear International Inc. BoartLongyear Corporation (CPN), Concord, California, USA). These data were gathered at six depths for each sampling location (0.1 m to 0.6 m in 0.1 m intervals). Figure1.2 shows a plan view where nine neutron probe access tubes for soil moisture measurements were installed in the solar area. Three access tubes were installed in each sub-treatment: SFO, SPO, and SFC respectively. Three access tubes were also installed in the control area. Neutron Probe readings were taken approximately every three days. A standard count was taken prior to sampling each day to calibrate data readings. Three neutron counts were averaged for each individual measurement (a single depth in a single tube). This count was normalized by the standard count, and the normalized count was calibrated to soil moisture. Within each sub-treatment, data at the same depths are averaged to determine the soil moisture profile and error-bars. The result is a soil moisture profile with measurements at 0.1, 0.2, 0.3, 0.4, 0.5, and 0.6 m for each sub-treatment and the control every three days. Neutron probe readings at the 0.1m depth for all sub-treatments and the control were adjusted to account for possible neutron losses to the atmosphere (Parkes & Siam, 1979). Two-way ANOVA was used to test the independence of the soil moisture measurements with respect to zoning (the control, SFO, SPO, and SFC) and depth. Time series of the soil moisture at 0.2 m, 0.4 m and 0.6 m are presented in Figure 1.4 in subpanels a-c. Time series of soil moisture at 0.1 m, 0.3 m and 0.5 m can be found in Appendix B.

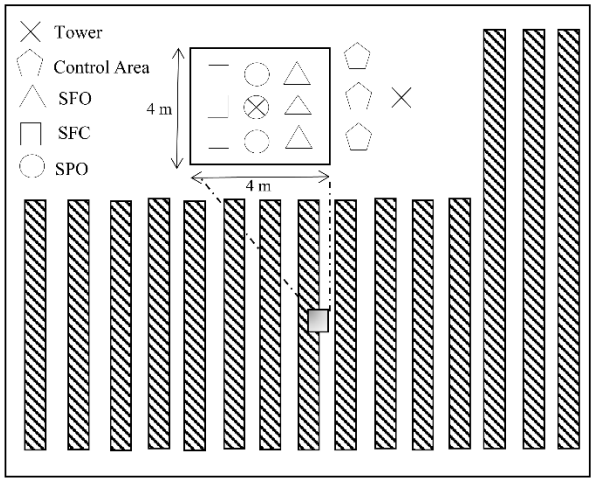

Figure1.2 Plan view of experimental setup in solar array area showing locations of towers and neutron probe access tubes for: Solar Fully Covered (SFC), Solar partially open (SPO), Sky Fully Open (SFO), solar measurements are almost 70 meters apart from control area

Biomass measurements

Above-ground biomass was collected on the 28th of August. Six 1m by 1m quadrants were collected from within the fenced areas for each sub-treatment and the control. Harvested biomass was dried for 48 hours in a 105 ^{o}C oven and weighed. The Daubenmire method [10] was used to study grass species diversity at the end of July. Six transects in the control and one transect in the solar array were performed. For each transect, a random number was drawn (from 1-10) to determine the final location of each 1m x1m quadrant. Six quadrants were collected in each transect resulting in a total of 42 samples. In each quadrant, the coverage, by species, was determined visually.

1.5 Results and Discussions

Micrometeorological variables

Using a Kolmogorov Smirnov test, a two tailed t-test, standard deviation and William Watson test(Berens, 2009) for wind direction showed subtle but statistically significant differences. Significant differences in mean temperature were found in readings taken closest to the PV panel surfaces at the 1.2 m and 2.0 m elevations. No significant

differences were observed at the lowest (0.5 m) or highest (2.7 m) elevations. Note that the magnitude of these mean temperature differences are smaller than those reported from simulation studies [5-8]. Significant differences in mean relative humidity and wind speed were found for all measurement heights. Solar radiation below the solar panel installation height was significantly reduced (as expected) and the incoming solar radiation measured at a height above the solar panels was found to be statistically significant (unexpected) but the difference relatively small. The distribution of wind direction was significantly altered at all heights, and the mean wind speed was significantly different at all heights. A summary of the p-values from all statistical tests is shown in Table 1.1. Standard deviation values were big due to diurnal changes of micro climate variables during the day.

Table 1. 1 Mean/Std and p-values from solar panel and control area Two-sample Kolmogorov-Smirnov, t tests and William Watson test

Elevation (m)		**0.5**	**1.2**	**2.0**	**2.7**
Temperature (°C)	Mean/Std (solar panel area)	18.34/7.87	18.03/8.06	18.30/7.39	18.37/7.65
	Mean/Std (control area)	18.27/7.85	18.32/8.31	18.36/7.47	18.11/7.64
	p-values (KS test)	0.9964	0.9964	1.0000	1.0000
	p-values (t test)	0.1527	**0.0000**	**0.0000**	0.5996
Relative humidity (%)	Mean/Std (solar panel area)	65.62/0.226	64.17/0.252	64.29/0.209	64.92/0.230
	Mean/Std (control area)	66.23/0.234	66.38/0.242	64.89/0.222	65.37/0.223
	p-values (KS test)	**0.0004**	0.3611	0.7014	0.6703
	p-values (t test)	**0.0000**	**0.0000**	**0.0000**	**0.0118**
Wind speed (m/s)	Mean/Std (solar panel area)	0.5471/0.506	0.4880/0.427	1.3777/1.083	1.0889/0.909
	Mean/Std (control area)	0.8752/0.665	0.6384/0.520	1.1313/0.859	0.9726/0.757
	p-values (KS test)	0.9579	1.0000	0.8497	0.9964
	p-values (t test)	**0.0000**	**0.0000**	**0.0000**	**0.0000**

Solar radiation (W/m2)	Mean/Std (solar panel area)	-	59.53/96.65	-	275.72/322.59
	Mean/Std (control area)	-	328.26/407.93	-	271.58/323.34
	p-values (KS test)	-	**0.0099**	-	0.9597
	p-values (t test)	-	**0.0000**	-	**0.0054**
Wind direction (°)	Mean/Std (solar panel area)	196.29/107.71	220.96/102.32	211.83/101.68	206.11/96.65
	Mean/Std (control area)	210.54/102.29	196.82/121.16	211.87/95.91	182.13/115.97
	p-values (WW test)	**0.0000**	**0.0000**	**0.0000**	**0.0000**

Wind direction data at 2.7 m above ground level is shown in Figure 1.3 to illustrate the alterations in the wind direction. For the sake of brevity, only one height is presented in this manuscript, but all heights are shown in Appendix A. Figure1.3 shows a histogram of incident wind direction plotted as a function of direction. Longer spokes indicate that that particular direction is more probable. Each spoke is divided and colored according to the strength of the wind (wind speed). For example, a long blue spoke would indicate that light winds from that direction are common. We can conclude from Figure 1.3 that the wind direction in the control area is distributed among many incident angles, while the wind direction within the treatment is oriented predominantly from the south. That is, the wind direction within the treatment area reorients with solar panels such that the wind is from south to north. The panels do not act as 'canyons' and orient the wind along their rows (a common occurrence in urban flows for example)(Pavageau & Schatzmann, 1999). Rather, the wind is reoriented perpendicular to the solar array's rows. The authors believe that the local increase in temperature near the solar panel surface results in a buoyant force that causes local anabatic flow up the panel surfaces. Each anabatic flow on each PV row has a vector component perpendicular to the solar panel row orientation, and the entire solar farm acts like a 'Fresnel slope' that reorients the flow. The total buoyant force is enough to accelerate the flow directionally, and contributes the increase in wind speed above the

panels. Flow acceleration around a bluff body (PV panel) also contributes to increased wind speed above the solar panels. Increased drag due to the 'solar canopy' is likely the cause of the reduced speed below the solar panels. Note that the most common wind speeds are weak (<2m/s), and it is unclear if this wind direction shift would be a robust result for windy locations. Higher wind speeds are also observed to reorient in Figure 1.3; however, the number of occurrences are limited.

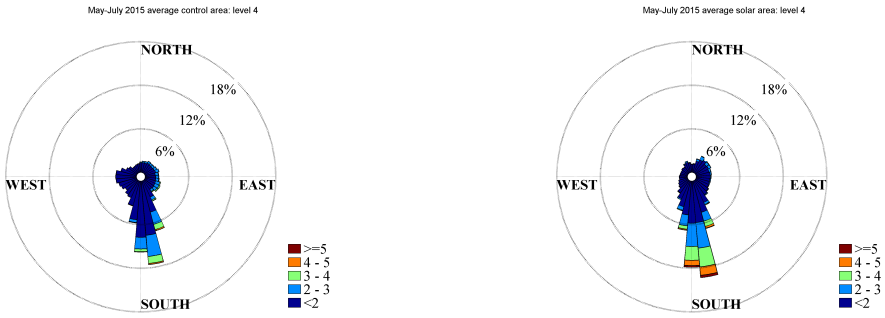

(a) (b)

Figure1. 1 Wind rose plots for control (left) and solar areas (right) for May-August average wind directions. The data are for elevation 2.7 m

Soil moisture data comparisons

The horizontal axis shows the Day of Year (DoY) of the data collection in 2015 and vertical axis is the volumetric soil moisture in vol/vol. Independence was determined with a p-value of less than 0.01 for all depths and zones by two-way ANOVA test. The soil moisture is near saturation for all depths and all treatments at the start of observation. That is, all areas had nearly identical initial soil moistures. The differing rates of soil water depletion in the three sub-treatments and the control led to dramatic differences in late season soil moisture.

The soil moisture in the SFO area is depleted more rapidly than the SPO, SFC or control areas. This result is intriguing since the SFO area and the control experience similar

incident solar radiation. Thus, the SFO must have a different energetic balance despite similar exposure to direct solar energy. We hypothesize that this difference in rate of soil moisture loss is a result of the longwave radiation transfer. The SFO will experience incident long wave radiation from the adjacent PV panels. These PV panels would also reduce the sky view factor of the SFO area. In contrast, the sky view in the control area is unobstructed. Thus, we infer that the total net long wave and net shortwave radiation both play an important role in the energetics and evaporation in the SFO area. The complete long and short wave radiation budgets within an agrivoltaic system will be explored in future study.

Soil moisture is most persistent in the SFC area and remains available for a larger portion of the growing season. The soil moisture at 0.6 m depth remained close to saturation (0.3 vol/vol) for the entire season which implies that water is available at the bottom of the root zone over the period of observation Figure 1.4 c. Overall the SFC area remained wetter than all other areas, including the control. This water availability is in stark contrast to the SFO area which was near saturation at the start of observation (~0.3 vol/vol) and depleted to ~0.2 vol/vol at the end of the season. This stark contrast in the moisture availability between the SFO and SFC creates an undesirable variability across the field and hints that shade uniformity may be an important consideration for the design of future agrivoltaic systems. The SPO area dries at a rate slower than the SFO but faster than the SFC and the control.

In other words, for most times and soil depths, the SFC had that highest soil moisture followed by the SPO, control and SFO respectively. It should be noted that the mean soil moisture across the SPO, SFO and SFC regions is similar to the control. But, the solar panels increase the local heterogeneity of soil water conditions, which results in some areas (SFC) having more persistent stores of soil water throughout the growing season.

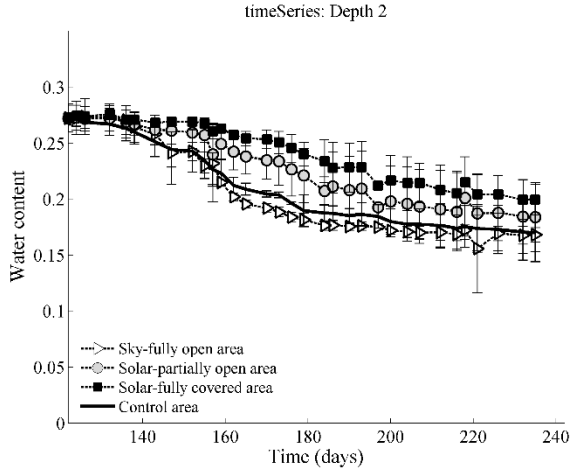
timeSeries: Depth 2
Water content
Time (days)
Sky-fully open area
Solar-partially open area
Solar-fully covered area
Control area

(a)

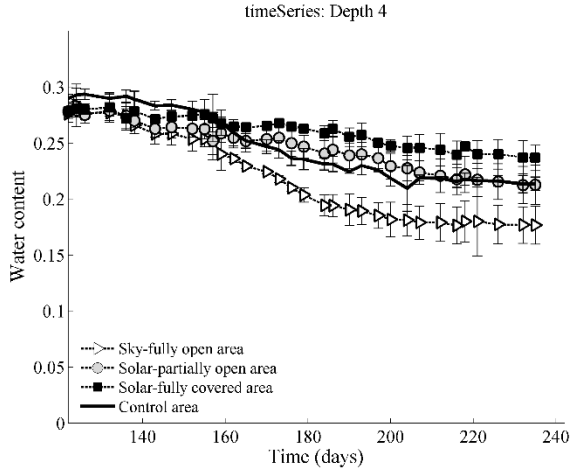
timeSeries: Depth 4
Water content
Time (days)
Sky-fully open area
Solar-partially open area
Solar-fully covered area
Control area

(b)

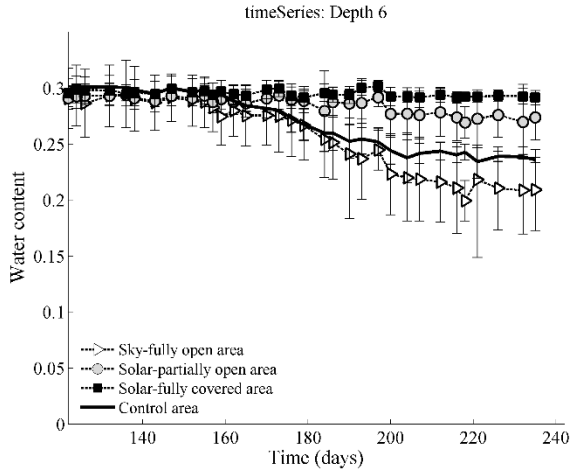
timeSeries: Depth 6
Water content
Time (days)
Sky-fully open area
Solar-partially open area
Solar-fully covered area
Control area

(c)

Figure1. 2 Soil moisture time series (a) 0.2m, (b) 0.4m and (c) 0.6m. For more information: there was 40 mm precipitation over the observation period, i.e. May-Aug 2015

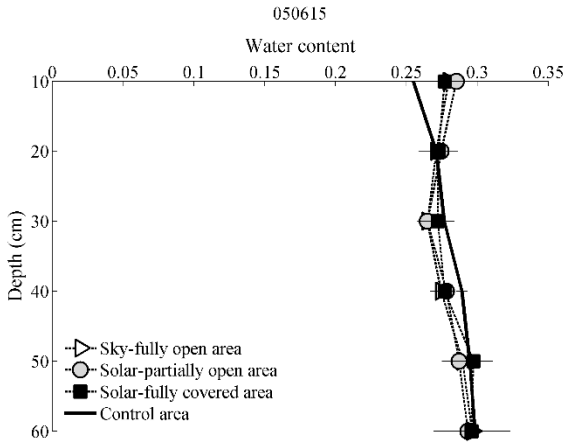

(a)

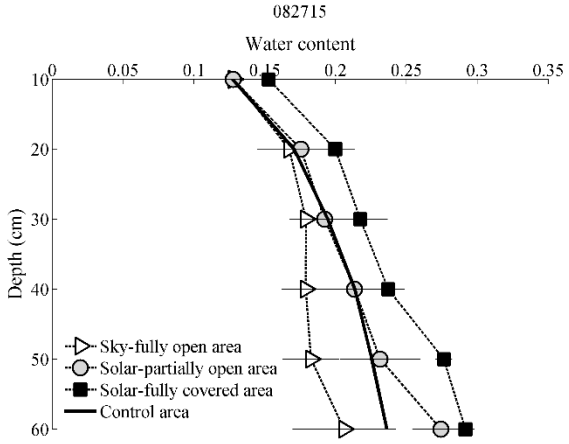

(b)

Figure1. 3 selected normalized soil moisture profiles from data sampling to show the change in soil moisture through growing season, (a) May 06-2015 and (b) August 27-2015.

The soil profiles at the beginning and end of the observation period are shown in Figure 1.5 All areas were near saturation for all depths initially. By the end of the observation period, the soil moisture in the SFC zone was nearly twice the SFO. These measurements are separated by less than two meters spatially. All measured soil moisture profiles are available in Appendix C.

Vegetation

Eight grass types were identified in the control pasture and five were identified in the solar farm area. A summary of the results is presented in Table 1.2. The most common species in the solar panel area was Alopecurus, a long-lived perennial that thrives in moist conditions. Alopecurus provides a "succulent and palatable forage" (W.M. Murphy, 1976). The most prevalent grass type in control area is Hordeum that has spikelet clusters that can enter nostrils and ear canals in mammals. Three types of grasses Calamagrostis, Cirsium and Dactylis were observed only in the control area. These grasses are only favored by sheep and cattle in the early stage of the grass before spine develops (De Bruijn & Bork, 2006). The causal factor for the diversity change between control and treatment requires further investigation.

Table 1. 2 The results of biomass monitoring for different grass types in solar and control area.

Grass scientific name (common name)	Solar area (%)	Control area (%)
Hordeum (Foxtail barely)	10	25
Agrostis (Redtop bentgrass)	30	20
Alopecurus (Meadow foxtail)	50	7
Schedonorus (Tall rye grass)	5	9
Bromus (Foxtailbrome)	5	22
Calamagrostis (Reed grass)	0	6
Cirsium (Thistle)	0	10.5
Dactylis (Orchard grass)	0	0.5

The harvested dry biomass at the end of the observation period is shown in Figure1.6 Results show 126% more dry biomass in the SFC zone relative to the SFO zone and 90% more dry biomass in the SFC zone relative to the control. Although the sample size is small, difference between the SFC and the control were found to be significant, (p-value=0.007). In addition, the difference between the SFC and the SFO were found to be significant, (p-value=0.007).

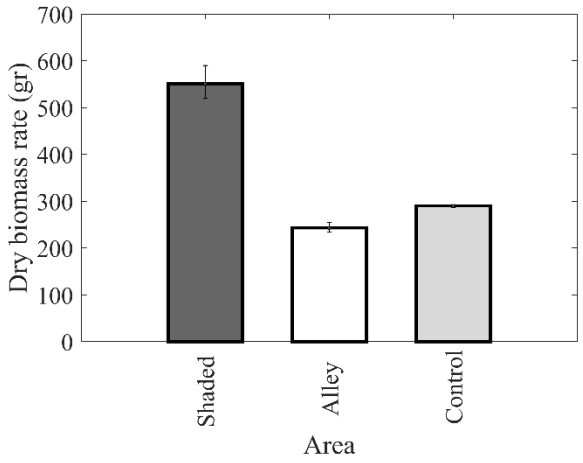

Figure1. 4 Dry biomass comparison in three places Solar Fully Covered (SFC), Sky Fully Open (SFO) and control area

Water Usage

Water usage was calculated based on difference in depth averaged soil moisture between the beginning (Figure 1.5(a) and end (Figure 1.5(b)) of the observation period. Averages are calculated by integrating soil moisture over soil depth from 10cm to 60cm. Water Use Efficiency (WUE) is then calculated as the biomass produced per unit of water used. Water use efficiencies in kg biomass/m^3 of water against the biomass weight in control and SFO and SFC treatments are presented in Figure 1.7 ($\frac{\text{WUE SFC} - \text{WUE Control area}}{\text{WUE Control area}}$). The higher producing SFC treatment was also significantly more water efficient (328%).

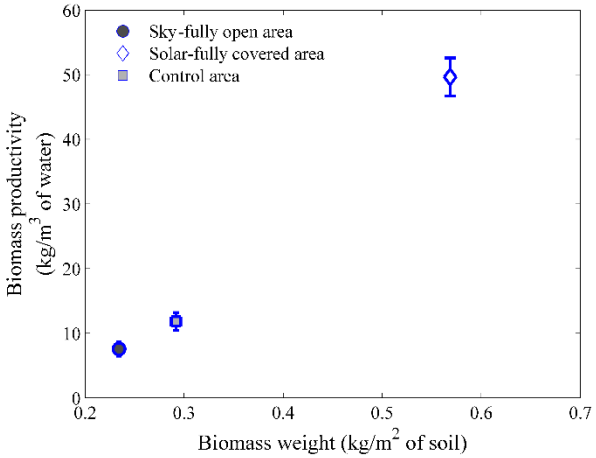

Figure1. 5 Biomass productivity in kg/ m^3 of water

The seasonal climate pattern at the site produces an initially saturated pasture and a a dry growing season. Initial water stores are depleted, through evapotranspiration (ET), and water scarcity occurs in the control and SFO areas. The shaded treatments (SFC and SPO) experience lower potential evapotranspiration (PET) due to decreased solar radiation throughout the observation period which resulted in a slower dry-down of the stored soil water. The decreased rate of dry-down in the SFC and SPO areas left soil water stores available throughout the observation period and allowed pasture grasses in the SFC and SPO to accumulate a significantly greater biomass. The reduced PET in the SFC and SPO treatments also contributed to an increase in water use efficiency of the pasture grasses. That is, a 'water limited' area, in a Budyiko (Budyko, 1971) sense, could be considered as an area of 'solar excess.' By harvesting this solar excess with solar panels, PET is reduced. Taken to an extreme it is possible to shift the aridity such that the shaded area becomes energy limited. Thus there must exist a shading level, for a water limited area, where PET and AET would be in balance. . We would not expect a similar outcome in 'energy limited' areas (Budyko sense) as observed by Armstrong et al. (Armstrong et al., 2016). In this case, there is no solar excess and the PET is already equal to the AET. If solar arrays were placed above growing plants in 'energy limited' conditions we would expect that the total biomass production would decrease, consistent with the findings of Armstrong et al. [16].

1.6 Conclusion

Typical agricultural operations manage multiple on-farm resources including soil, nutrients and water. This study suggests that the on-farm solar resource management could also be implemented for productive benefits. Water limited areas are most likely to benefit as solar management reduces PET and consequently the water demand. Not all crops will be amenable to solar management, and the economics of active solar management with PV panels needs further study. But, semi-arid pastures with wet winters may be ideal candidates for agrivoltaic systems as supported by the dramatic gains in productivity (90%) observed over the May-Aug 2015 observation period at the Rabbit Hills agrivoltaic solar array. These net benefits were largely achieved through

an increased water use efficiency in the shaded areas of the field which left water stored in the soil column available throughout the entire observation period. Extreme heterogeneity and spatial gradients in biomass production and soil moisture were observed as a result of the heterogeneous shade pattern of the PV array. Future agrivoltaic designs should eliminate this heterogeneity by optimizing PV panel placement to create a spatially uniform shadow pattern. A spatially uniform shadow pattern would foster uniform biomass accumulation benefits. The agricultural benefits of energy and pasture co-location could reduce land competition and conflict between renewable energy and agricultural production. Reduced or eliminated land completion would open new areas for PV installation. Local climatic effects of agrivoltaic installations were statistically significant but subtle, however the regional climatic impacts (e.g. rainfall patterns) of large scale agrivoltaic instillations are still unclear and should be the subject of further study.

1.7 Acknowledgment

Sincere acknowledgment is addressed to Dr. Ziru Liu (Postdoc in NewAg lab) for field assistance.

1.8 References

Al- Sabounchi, A. M. (1998). Effect of ambient temperature on the demanded energy of solar cells at different inclinations. *Renewable Energy*, *14*(1), 149–155. https://doi.org/10.1016/S0960-1481(98)00061-5

Allen, R. G., Tasumi, M., & Trezza, R. (2007). Satellite-based energy balance for mapping evapotranspiration with internalized calibration (METRIC)—Model. *Journal of Irrigation and Drainage Engineering*, *133*(4), 380–394.

Appelbaum, J., & Bany, J. (1979). Shadow effect of adjacent solar collectors in large scale systems. *Solar Energy*, *23*(6), 497–507.

Arán Carrión, J., Espín Estrella, A., Aznar Dols, F., Zamorano Toro, M., Rodríguez, M., & Ramos Ridao, A. (2008). Environmental decision-support systems for evaluating the carrying capacity of land areas: Optimal site selection for grid-connected photovoltaic power plants. *Renewable and Sustainable Energy Reviews*, *12*(9), 2358–2380. https://doi.org/10.1016/j.rser.2007.06.011

Armstrong, A., Ostle, N. J., & Whitaker, J. (2016). Solar park microclimate and vegetation management effects on grassland carbon cycling. *Environmental Research Letters*, *11*(7), 74016.

Barron-Gafford, G. A., Minor, R. L., Allen, N. A., Cronin, A. D., Brooks, A. E., & Pavao-Zuckerman, M. A. (2016). The Photovoltaic Heat Island Effect: Larger solar power plants increase local temperatures. *Scientific Reports*, *6*, srep35070. https://doi.org/10.1038/srep35070

Berens, P. (2009). CircStat: a MATLAB toolbox for circular statistics. *J Stat Softw*, *31*(10), 1–21.

Broxton, P. D., Zeng, X., Sulla-Menashe, D., & Troch, P. A. (2014). A global land cover climatology using MODIS data. *Journal of Applied Meteorology and Climatology*, *53*(6), 1593–1605.

Budyko, M. I. (Mikhail I. (1971). Climate and life. Retrieved from http://agris.fao.org/agris-search/search.do?recordID=US201300494263

Calaf, M., Parlange, M. B., & Meneveau, C. (2011). Large eddy simulation study of scalar transport in fully developed wind-turbine array boundary layers. *Physics of Fluids (1994-Present)*, *23*(12), 126603.

Charabi, Y., & Gastli, A. (2011). PV site suitability analysis using GIS-based spatial fuzzy multi-criteria evaluation. *Renewable Energy*, *36*(9), 2554–2561.

Chu, S., & Majumdar, A. (2012). Opportunities and challenges for a sustainable energy future. *Nature*, *488*(7411), 294.

Dai, K., Bergot, A., Liang, C., Xiang, W.-N., & Huang, Z. (2015). Environmental issues associated with wind energy – A review. *Renewable Energy*, *75*, 911–921. https://doi.org/10.1016/j.renene.2014.10.074

De Bruijn, S. L., & Bork, E. W. (2006). Biological control of Canada thistle in temperate pastures using high density rotational cattle grazing. *Biological Control*, *36*(3), 305–315.

Dinesh, H., & Pearce, J. M. (2016). The potential of agrivoltaic systems. *Renewable and Sustainable Energy Reviews*, *54*, 299–308. https://doi.org/10.1016/j.rser.2015.10.024

Dupraz, C., Marrou, H., Talbot, G., Dufour, L., Nogier, A., & Ferard, Y. (2011a).

Combining solar photovoltaic panels and food crops for optimising land use: Towards new agrivoltaic schemes. *Renewable Energy*, *36*(10), 2725–2732. https://doi.org/10.1016/j.renene.2011.03.005

Dupraz, C., Marrou, H., Talbot, G., Dufour, L., Nogier, A., & Ferard, Y. (2011b). Combining solar photovoltaic panels and food crops for optimising land use: Towards new agrivoltaic schemes. *Renewable Energy*, *36*(10), 2725–2732. https://doi.org/10.1016/j.renene.2011.03.005

Dupraz, C., Talbot, G., Marrou, H., Wery, J., Roux, S., Liagre, F., et al. (n.d.). To Mix or Not to Mix: Evidences for the Unexpected High Productivity of New Complex Agrivoltaic and Agroforestry Systems. 2011. *Available Onlin E: Https://Www. Researchgate. Net/Publication/230675951_To_ Mix_or_not_to_mix__evidences_for_the_unexpected_high_productivity_of_new_com plex_agrivoltaic_ And_agroforestry_systems (Accessed on 9 December 2015)*, 202–203.

Dupré, O., Vaillon, R., & Green, M. A. (2016). *Thermal behavior of photovoltaic devices: physics and engineering*. Springer.

EarthExplorer. (n.d.). Retrieved March 1, 2018, from https://earthexplorer.usgs.gov/

Hassanpour Adeh, E., Higgins, C. W., & Selker, J. S. (2017). Remarkable solar panels Influence on soil moisture, micrometeorology and water-use efficiency. Retrieved from https://ir.library.oregonstate.edu/xmlui/handle/1957/60846

Higgins, C. W., Vache, K., Calaf, M., Hassanpour, E., & Parlange, M. B. (2015). Wind turbines and water in irrigated areas. *Agricultural Water Management*, *152*, 299–300. https://doi.org/10.1016/j.agwat.2014.11.016

Hu, A., Levis, S., Meehl, G. A., Han, W., Washington, W. M., Oleson, K. W., et al. (2016). Impact of solar panels on global climate. *Nature Climate Change*, *6*(3), 290–294. https://doi.org/10.1038/NCLIMATE2843

Huld, T., & Amillo, A. M. G. (2015). Estimating PV module performance over large geographical regions: The role of irradiance, air temperature, wind speed and solar spectrum. *Energies*, *8*(6), 5159–5181.

Kadowaki, M., Yano, A., Ishizu, F., Tanaka, T., & Noda, S. (2012). Effects of greenhouse photovoltaic array shading on Welsh onion growth. *Biosystems*

Engineering, *111*(3), 290–297. https://doi.org/10.1016/j.biosystemseng.2011.12.006

Kratochvil, J. A., Boyson, W. E., & King, D. L. (2004). *Photovoltaic array performance model.* Sandia National Laboratories.

Krauter, S. (2004). Increased electrical yield via water flow over the front of photovoltaic panels. *Solar Energy Materials and Solar Cells*, *82*(1–2), 131–137.

Lewis, N. S., & Crabtree, G. (2005). *Basic research needs for solar energy utilization: report of the basic energy sciences workshop on solar energy utilization, April 18-21, 2005*. US Department of Energy, Office of Basic Energy Science.

Lewis, N. S., & Nocera, D. G. (2006). Powering the planet: Chemical challenges in solar energy utilization. *Proceedings of the National Academy of Sciences*, *103*(43), 15729–15735. https://doi.org/10.1073/pnas.0603395103

Li, X., Wagner, F., Peng, W., Yang, J., & Mauzerall, D. L. (2017). Reduction of solar photovoltaic resources due to air pollution in China. *Proceedings of the National Academy of Sciences*, *114*(45), 11867–11872. https://doi.org/10.1073/pnas.1711462114

Lin, C., Yang, K., Huang, J., Tang, W., Qin, J., Niu, X., et al. (2015). Impacts of wind stilling on solar radiation variability in China. *Scientific Reports*, *5*. https://doi.org/10.1038/srep15135

Marrou, H., Dufour, L., & Wery, J. (2013). How does a shelter of solar panels influence water flows in a soil–crop system? *European Journal of Agronomy*, *50*, 38–51. https://doi.org/10.1016/j.eja.2013.05.004

Marrou, H., Wéry, J., Dufour, L., & Dupraz, C. (2013). Productivity and radiation use efficiency of lettuces grown in the partial shade of photovoltaic panels. *European Journal of Agronomy*, *44*, 54–66.

Mellit, A., & Pavan, A. M. (2010). Performance prediction of 20kWp grid-connected photovoltaic plant at Trieste (Italy) using artificial neural network. *Energy Conversion and Management*, *51*(12), 2431–2441. https://doi.org/10.1016/j.enconman.2010.05.007

Millstein, D., & Menon, S. (2011). Regional climate consequences of large-scale cool roof and photovoltaic array deployment. *Environmental Research Letters*, *6*(3), 34001.

Muradov, N. Z., & Veziroğlu, T. N. (2008). “Green” path from fossil-based to

hydrogen economy: an overview of carbon-neutral technologies. *International Journal of Hydrogen Energy*, *33*(23), 6804–6839.

Nonhebel, S. (2005). Renewable energy and food supply: will there be enough land? *Renewable and Sustainable Energy Reviews*, *9*(2), 191–201.

Noorollahi, E., Fadai, D., Akbarpour Shirazi, M., & Ghodsipour, S. H. (2016). Land suitability analysis for solar farms exploitation using GIS and fuzzy analytic hierarchy process (FAHP)—a case study of Iran. *Energies*, *9*(8), 643.

Obama, B. (2017). The irreversible momentum of clean energy. *Science*, *355*(6321), 126–129. https://doi.org/10.1126/science.aam6284

On the temperature dependence of photovoltaic module electrical performance: A review of efficiency/power correlations - ScienceDirect. (n.d.). Retrieved August 17, 2017, from http://www.sciencedirect.com/science/article/pii/S0038092X08002788

Parkes, M. E., & Siam, N. (1979). Error associated with measurement of soil moisture change by neutron probe. *Journal of Agricultural Engineering Research*, *24*(1), 87–93.

Pavageau, M., & Schatzmann, M. (1999). Wind tunnel measurements of concentration fluctuations in an urban street canyon. *Atmospheric Environment*, *33*(24–25), 3961–3971.

Pookpunt, S., & Ongsakul, W. (2013). Optimal placement of wind turbines within wind farm using binary particle swarm optimization with time-varying acceleration coefficients. *Renewable Energy*, *55*, 266–276.

Porté-Agel, F., Wu, Y.-T., Lu, H., & Conzemius, R. J. (2011). Large-eddy simulation of atmospheric boundary layer flow through wind turbines and wind farms. *Journal of Wind Engineering and Industrial Aerodynamics*, *99*(4), 154–168.

PV-GIS: a web-based solar radiation database for the calculation of PV potential in Europe: International Journal of Sustainable Energy: Vol 24, No 2. (n.d.). Retrieved December 26, 2017, from http://www.tandfonline.com/doi/abs/10.1080/14786450512331329556

R. Saidur, N. A. R. (2011). Environmental impact of wind energy. *Renewable and Sustainable Energy Reviews*, *15*(5), 2423–2430. https://doi.org/10.1016/j.rser.2011.02.024

Ramachandra, T. V., & Shruthi, B. V. (2007). Spatial mapping of renewable energy

potential. *Renewable and Sustainable Energy Reviews*, *11*(7), 1460–1480. https://doi.org/10.1016/j.rser.2005.12.002

Ramli, M. A., Prasetyono, E., Wicaksana, R. W., Windarko, N. A., Sedraoui, K., & Al-Turki, Y. A. (2016). On the investigation of photovoltaic output power reduction due to dust accumulation and weather conditions. *Renewable Energy*, *99*, 836–844.

Ravi, S., Lobell, D. B., & Field, C. B. (2014). Tradeoffs and Synergies between Biofuel Production and Large Solar Infrastructure in Deserts. *Environmental Science & Technology*, *48*(5), 3021–3030. https://doi.org/10.1021/es404950n

Rodman, L. C., & Meentemeyer, R. K. (2006). A geographic analysis of wind turbine placement in Northern California. *Energy Policy*, *34*(15), 2137–2149.

Rogner, H. H., & others. (2012). *inGlobal Energy Assessment—Towards a Sustainable FutureCh. 7, 423–512*. Cambridge University Press.

Scherba, A., Sailor, D. J., Rosenstiel, T. N., & Wamser, C. C. (2011). Modeling impacts of roof reflectivity, integrated photovoltaic panels and green roof systems on sensible heat flux into the urban environment. *Building and Environment*, *46*(12), 2542–2551. https://doi.org/10.1016/j.buildenv.2011.06.012

Seidlova, L., Verlinden, M., Gloser, J., Milbau, A., & Nijs, I. (2009). Which plant traits promote growth in the low-light regimes of vegetation gaps? *Plant Ecology*, *200*(2), 303–318. https://doi.org/10.1007/s11258-008-9454-6

Shah, A., Torres, P., Tscharner, R., Wyrsch, N., & Keppner, H. (1999). Photovoltaic Technology: The Case for Thin-Film Solar Cells. *Science*, *285*(5428), 692–698. https://doi.org/10.1126/science.285.5428.692

Sheffield, J., Goteti, G., & Wood, E. F. (2006). c. *Journal of Climate*, *19*(13), 3088–3111. https://doi.org/10.1175/JCLI3790.1

Skoplaki, E., & Palyvos, J. A. (2009). On the temperature dependence of photovoltaic module electrical performance: A review of efficiency/power correlations. *Solar Energy*, *83*(5), 614–624.

The Fowler Ridge Wind Farm Project, USA. (n.d.). Retrieved May 11, 2018, from https://www.power-technology.com/projects/fowlerridgewindfarmi/

Trancik, J. E. (2014). Renewable energy: Back the renewables boom. *Nature*, *507*(7492), 300–302. https://doi.org/10.1038/507300a

Turner, J. A. (1999). A Realizable Renewable Energy Future. *Science*, *285*(5428), 687–689. https://doi.org/10.1126/science.285.5428.687

Web Soil Survey - Home. (n.d.). Retrieved June 5, 2017, from https://websoilsurvey.sc.egov.usda.gov/App/HomePage.htm

Weiss, D. N. (2018). Predicted: Photovoltaic Plant Performance. *Joule*, *2*(2), 199–200. https://doi.org/10.1016/j.joule.2018.01.016

When will fossil fuel reserves be diminished? - ScienceDirect. (n.d.). Retrieved November 15, 2017, from http://www.sciencedirect.com/science/article/pii/S0301421508004126

W.M. Murphy, M. . J. (1976). *Grass varieties for central Oregon* (Agricultural Experiment Station Oregon State University, Corvallis No. Special Report 468).

2. Chapter 2: Solar Power Potential Greatest Over Crop Lands

Elnaz Hassanpour Adeh[1], Stephen P Good[1], M. Calaf [2], Chad W. Higgins[*1]
[1] Department of Biological and Ecological Engineering, Oregon State University, Corvallis, USA
[2] Department of Mechanical Engineering, University of Utah, UT, USA
[*]Corresponding author, Email: chad.higgins@oregonstate.edu, Tel: +15417372286

2.1 Abstract

Solar energy is the fastest growing renewable energy source, and small changes in solar panel efficiency can have dramatic economic consequences. Though it is critical to understand the factors influencing solar efficiency for proper array operations, current studies largely ignore many environmental factors that influence photovoltaic panel function. In this paper, an energy balance model is constructed for photovoltaic panels which incorporates the environmental conditions. The model is then verified with field measurements that were obtained across a range of microclimate conditions. Results confirm that the photovoltaic panel efficiency is affected by the air temperature, wind speed and relative humidity, which suggests convective cooling and vapor pressure are also important factors. This model is applied globally using bias-corrected reanalysis datasets to map solar efficiency and potential solar power production considering the temperature, wind speed, radiation and relative humidity effects. Solar power production potential is then classified based on global land cover distributions. This analysis demonstrates that crop lands have the greatest median solar potential followed by grass land, and permanent wetlands. These results help decision makers to select the most appropriate land cover for future solar energy placement.

2.2 Main Manuscript

The goal of the United States Department of Energy (U.S. DOE) is to reach a levelized cost of energy for solar photovoltaics of $0.03 per kilowatt hour at utility scale by 2030 [1]. This objective will not only strengthen the U.S. economy and help the country reposition in the international energy market [2], but will also help reducing CO2 gas

emissions in view of climate change concerns [3]. In this regard, solar energy already represents a significant 1% share of the energy share in the U.S. and with the development of the Sunshot initiative [4] the goal is to enable solar energy to supply as much as ~ 30% of the U.S. electricity share by 2050 [5]. Assuming for an instant that this electricity was only to be generated by solar photovoltaics (PV, neglecting concentrated solar energy). As a result, it is not too far to envision a potential land competition between energy and food production [6] [7]as the total land area devoted to solar energy expands. It is for this reason that a detailed understanding of the available resources (e.g. solar radiation and land) and their corresponding overlapping use (e.g. energy, agricultural, or ecosystem services) is crucial[8] . The global expansion of solar energy in benefit of reducing current and future carbon footprints, will nonetheless require decisions on the most sustainable and effective energy infrastructure developments [9] as well as in regards to the locations of these developments. It is for this reason that one of the aims of this study is to augment the scientific grounds for this discussion by ranking land cover classes according to their solar energy production potential.

In the development of these new land cover classes, external forcing factors conditioning solar PV efficiency are well taken into consideration. For example, while solar PV fundamentally depends on the incoming solar radiation, which is a strong geographic-dependent function, it is also well known that the system's efficiency strongly depends on the temperature of the solar cells. Thermal losses in solar PV correspond to the reduction in electrical power output resultant of working at temperatures above 25 ◦C (Standard Test Conditions, STC) in which solar cells are developed and tested, as well as the associated accelerated aging. These thermal losses can be mitigated in the case of the mainstream crystalline silicon technology by: (1) cooling, through conduction/convection with a colder medium, and by radiation towards the surroundings and the cold outer space under clear sky conditions; (2) reduction of the thermal load or internal heat source in the panel; (3) minimizing the thermal sensitivity (temperature coefficient) of the electrical power output. While the first approach can be actively addressed by taking into consideration the influence of the surrounding medium (i.e. atmospheric flow, soil conditions, etc.), the other two are

technology dependent. Therefore, to develop the new land cover classes mentioned above, we first establish a first order physics- based model that links solar PV efficiency to four environmental forcing factors: air temperature, relative humidity, wind speed, and incoming solar radiation. This model incorporates the role of wind speed and air temperature on convective cooling and the effect of water vapor on the long wave radiation budget. This new simple model is evaluated using field data from a 1.5 MW solar array located at Oregon State University in Corvallis, Oregon. Upon validation, the reduced-order model is used to generate the land cover classes map that allow determining under what type of surfaces it would be more efficient to develop future solar energy projects.

2.3 Results

Figure 2.1 presents measurements of the solar PV efficiency as a function of (a) temperature, (b) wind speed, and (c) relative humidity, in comparison with measurements developed over a period of 4 months at the 1.5 MW solar farm located at Oregon State University, in Corvallis (OR). These results exclude night time periods as well as times of low sun angle. The boxes in Figure 2.1a illustrate the site-specific measured changes in solar PV efficiency as a function of temperature, illustrating a decrease in efficiency of almost 1% as median temperature increases by 20◦C. This is consistent with literature observations of deceased efficiency with increasing ambient temperature [10]. Alternatively, in Figure 2.1b, results indicate a median increase of about 0.5% with a change in wind speed from 0.5m/s to 3 m/s. This result is also in agreement with a recently published work of Dupre´ et al. [6] in which it is shown that small changes in the convective heat transfer coefficient, here induced by the increase in wind speed, can lead to significant changes in the solar PV efficiency. Last, the increase in vapor pressure also leads to a median reduction of 1%, illustrating the reduction in efficiency as relative humidity increases.

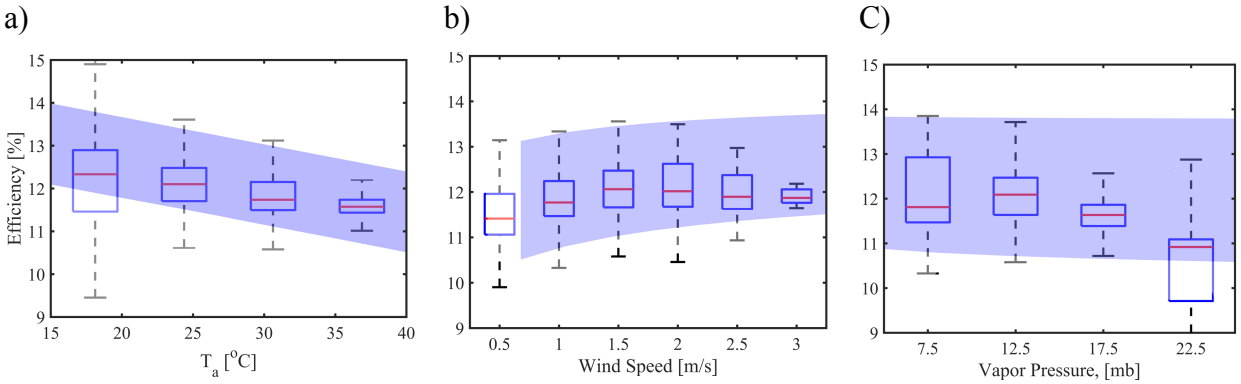

Figure 2. 1 Comparison of field data (box plots) and proposed model for Oregon State University solar arrays: a) air temperature, b) wind speed and c) vapor pressure

In parallel to the experimental measurements the parsimonious low-order model developed in this work (see the Methods section) is applied for the same study case only using local values of radiation, air temperature, humidity, and wind speed as inputs. The results in the solar PV system efficiency are represented by the shaded region, which in all cases overlaps well the experimental data.

Results of a global scale analysis

Upon validation of the newly developed low-order model, one can now use it to study the potential regions of the world, where implementing solar PV might be more efficient. For this purpose, the required inputs of solar radiation, air temperature, humidity and wind speed are obtained at a global scale from reanalysis products [11],[12]. The result is a global map of solar PV efficiency and solar power (see Figure 2.2) which provides a general overview of potential solar system installations. Results indicate that the most efficient continental locations include western America, southern Africa, and the Middle East. In this regard, it is also of value to observe the large discrepancies between different regions, hence emphasizing the relevance of this type of analysis prior to the development of large projects. Further, because both solar power and land cover are directly influenced by radiation, the model results were also conditionally sampled based on land cover type. This was identified using

NASAs Moderate Resolution Imaging Spectrometer (MODIS) [13]. As a result, seventeen land cover types were used, and their corresponding ranking in terms of associated median power potential was also computed. Croplands, grasslands, wetlands, mixed forest and barren land covers were the top five land classes (see Figure 2.3). Therefore, based on this analysis one can conclude that installing large arrays of solar PV panels on croplands is the most efficient based on the inputs of solar radiation, local temperature, averaged wind speed and relative humidity. In this regard, it is for example also very interesting to see how barren terrains, traditionally though as best for installation of solar PV systems, are only located in fifth place.

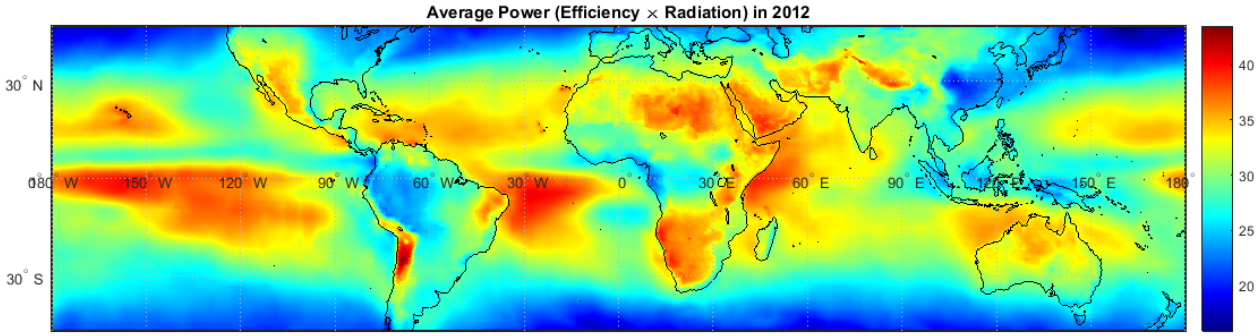

Figure 2. 2 Global map of potential solar power for climatic data calculated based on energy balance

This is because in these regions, at equal value of incoming solar radiation, near surface air temperature tends to be higher, and hence leading to the increase in temperature of the solar PV modules and decrease in overall efficiency. Similarly, in this study the relevance of solar radiation absorption by atmospheric water content (relative humidity) is also brought into relevance, as it can be for example observed by the lower efficiency found in the regions covered by snow and ice. Therefore, it is safe to conclude that the ideal site for solar PV energy harvesting should have important values of solar irradiance, with low near surface temperature values, moderate winds that would not transport dust or other types of aerosol, and with weak values of relative humidity.

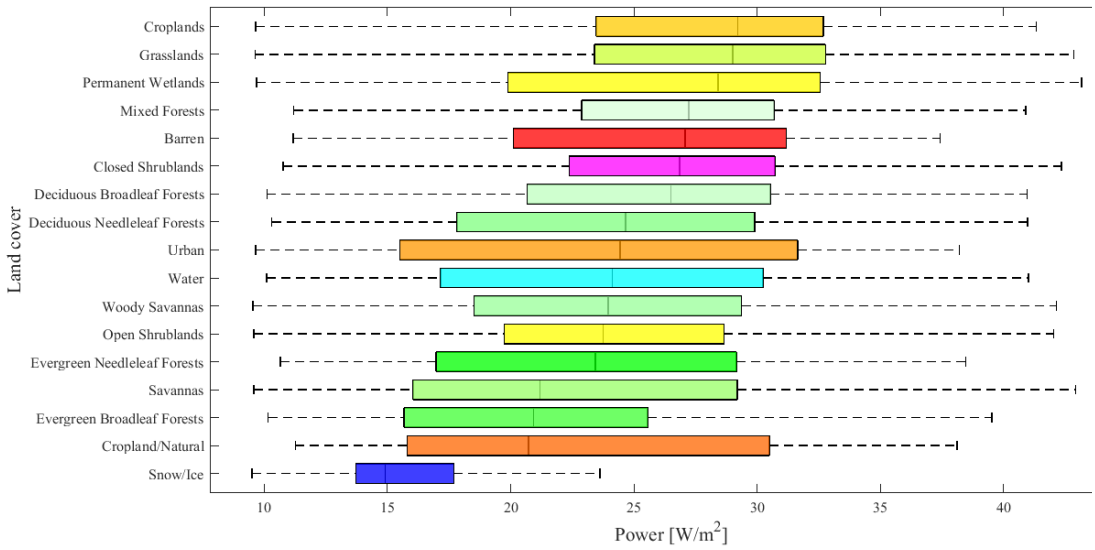

Figure 2. 3 Solar power potential ranked by Land cover classification

2.4 **Discussion**

Based in the results presented herein, it is suggested that there is the potential for land competition between land dedicated to food production versus land dedicated to efficient solar PV systems. Therefore, this unwanted competition may become a real issue, playing an important role in the near future of the water, energy, and food nexus. It is for this reason that climatic reasons derived from the developed low-order PV model strongly motivate the development of new management solutions such as solar sharing or agrivoltaic schemes. In this regard, Agrivoltaic systems leverage the superposition of energy and food production for mutual benefit. The authors believe that this could be a solution to the near-future crossroad given the appropriate technology is developed and the appropriate support of all stakeholders.

2.5 **Material and methods**

Data sources

Field data used in this study were collected during a two-year study on a six acre agrivoltaic solar farm and sheep pasture at Oregon State University Campus

(Corvallis, Oregon, US.)[12] . Climatic variables (T, RH, V, R) were collected at a height of two meters and at one minute intervals for two years using (DS-2) and (VP-3) Decagon Devices.

Low-order solar PV efficiency model definition

The low-order solar PV efficiency model is developed using an energy balance approach around a standard solar PV module. The energy balance is based on the first law of thermodynamics, and requires that the sum of the incoming energy to the solar module equals the outgoing energy from the solar module plus the thermally stored energy in the solar module. Figure 2.4 presents a schematic representation of the energy balance in the control volume.

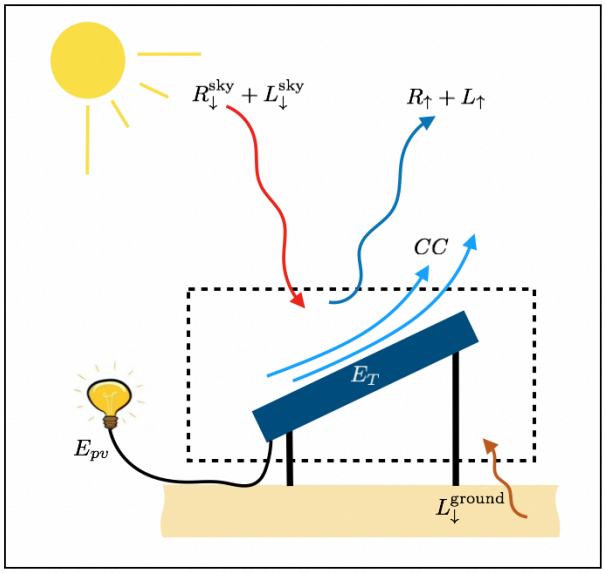

Figure 2.4: Graphical sketch illustrating the different components considered in the energy budget based low-order model.

The incoming energy is composed of the shortwave (R^{sky}) and longwave (L^{sky}) radiation coming from the sun as well as ↓↓ the incoming longwave radiation coming from the ground (L^{ground}). It is important to note that the incoming longwave ↓ radiation refers here to the integral longwave radiation reaching the solar module from the sky, which includes solar longwave radiation as well as longwave radiation emitted from nearby clouds or other reflecting objects besides the ground. Alternatively, the outgoing

energy is composed of a reflected shortwave component (R↑), an outgoing long wave component (L↑), the convective cooling (CC), and the final electrical energy (Epv). This can be expressed mathematically as follows,

$R^{sky} + L^{sky} + L^{ground} = R + L + CC + E_{pv} + E_T$

Where E_T represents the gain or loss of stored thermal energy expressed through a change of the panel's temperature. In the model, each specific terms is computed as follows,

$L^{sky} = 1.24\ \sigma\left(\frac{e_a}{T_a}\right)^{\frac{1}{7}} T_a^{\,4}$, $L^{ground} = \sigma\ T_{ground}$, $R = \alpha\ R^{sky}$, $L = 2\ \sigma T_p^{\,4}$, $E_{pv} = \varepsilon\ R^{sky}$, $CC = 2\ h\ (T_p - T_a)$ (2)

Where the convective heat transfer coefficient has been computed as $h=0.036\frac{k_{air}}{l_{panel}}\left(\frac{u(z)\ l_{panel}}{\upsilon}\right)^{4/5} P_r^{\,1/3}$ for an inclined flat plate. In the above expressions, $\sigma = 5.670367\times10^{-8}$ kg s^{-1} K^{-4} is the Stephan-Boltzman constant, ea is the pressure of water vapor, Ta, T_{ground}, and T_p indicate the air, ground and panel temperature correspondingly. Further ε is the efficiency of the solar panel, and α is the albedo. To keep the model simple, and as a first order approximation, the atmosphere is modeled under a neutral stratification, and only a steady state regime is considered. For this purpose, it is considered that the panel reaches thermal equilibrium very quickly, and hence ET is neglected. To compute the local convective heat transfer coefficient (used to account for the convective cooling), the model uses the local air temperature, and wind speed as indicated in equations 2. Further, the ambient air temperature and partial pressure of water vapor are also used to modify the long wave radiation budget. Finally, for each steady state configuration, equation 1 is solved for the efficiency of the system, ε. Assumptions and equations are summarized in table 1 and table 2.

Table 1| Assumptions for the energy balance model		
albedo = 0.2	A = 0.005	e_ref = 0.135
sigma = 5.67e-8	l_panel = 1.5	Pr = 0.707

nu = 1.57e-5	T_ref = 25+273;	E=e_ref*(1-A*(T_p-T_ref));
h=0.036.*k_air./l_panel.*(u.*l_panel./nu).^(4/5).*Pr^(1/3)		

Table 1| Incoming and outgoing energy for a photovoltaic panel

No	Incoming	Formulation	Outgoing	Formulation
1	Shortwave from sun	R	Reflected shortwave	α R
2	Longwave from sun	$1.24\ \sigma\left(\frac{e_a}{T_a}\right)^{\frac{1}{7}} {T_a}^4$	Electrical energy	ε R
3	Longwave from ground	$\sigma\ {T_g}^4$ $T_a(z) = T_g$	Outgoing long wave	$2\ \sigma\ {T_p}^4$
4			Convective cooling	$2\ h\ (T_p - T_a)$ $h=0.036\frac{k_{air}}{l_{panel}}\left(\frac{u(z)\ l_{panel}}{\upsilon}\right)^{4/5} {P_r}^{1/3}$ $u(z) = ku_* \ln\left(\frac{z}{z_o}\right)$

2.6 References

1. Providing all global energy with wind, water, and solar power, Part II: Reliability, system and transmission costs, and policies - ScienceDirect. Available at: https://www.sciencedirect.com/science/article/pii/S0301421510008694. (Accessed: 28th November 2018)
2. Stern, N. The economics of climate change. *Am. Econ. Rev.* **98**, 1–37 (2008).
3. Olah, G. A. Beyond oil and gas: the methanol economy. *Angew. Chem. Int. Ed.* **44**, 2636–2639 (2005).

4. Opportunities and challenges for a sustainable energy future | Nature. Available at: https://www.nature.com/articles/nature11475. (Accessed: 28th November 2018)

5. Williams, J. H. *et al.* The technology path to deep greenhouse gas emissions cuts by 2050: the pivotal role of electricity. *science* **335**, 53–59 (2012).

6. Dupraz, C. *et al.* Combining solar photovoltaic panels and food crops for optimising land use: Towards new agrivoltaic schemes. *Renew. Energy* **36**, 2725–2732 (2011).

7. Valentine, J. *et al.* Food vs. fuel: the use of land for lignocellulosic 'next generation'energy crops that minimize competition with primary food production. *Gcb Bioenergy* **4**, 1–19 (2012).

8. Energy transitions and the global land rush: Ultimate drivers and persistent consequences - ScienceDirect. Available at: https://www.sciencedirect.com/science/article/abs/pii/S0959378011002068. (Accessed: 29th November 2018)

9. Omer, A. M. Energy, environment and sustainable development. *Renew. Sustain. Energy Rev.* **12**, 2265–2300 (2008).

10. Al- Sabounchi, A. M. Effect of ambient temperature on the demanded energy of solar cells at different inclinations. *Renew. Energy* **14**, 149–155 (1998).

11. Remarkable agrivoltaic influence on soil moisture, micrometeorology and water-use efficiency. Available at: https://journals.plos.org/plosone/article?id=10.1371/journal.pone.0203256. (Accessed: 29th November 2018)

12. Hassanpour Adeh, E., Higgins, C. W. & Selker, J. S. Remarkable solar panels Influence on soil moisture, micrometeorology and water-use efficiency-database. (2017).

13. Broxton, P. D., Zeng, X., Sulla-Menashe, D. & Troch, P. A. A global land cover climatology using MODIS data. *J. Appl. Meteorol. Climatol.* **53**, 1593–1605 (2014).

2.7 Acknowledgements

E.H. acknowledges support from the USDA United States department of Agriculture (OREZ-FERM-852-E) and NSF (EAR – 1740082).

2.8 Author Contributions

E.H and C.W.H conceived the study with inspiration from M.C and S.P.G. E.H performed the analyses and mainly wrote the manuscript. All contributed to discussion and the manuscript.

2.9 Author Information

Reprints and permissions information is available at www.nature.com/reprints. The authors declare no competing financial interests. Readers are welcome to comment on the online version of the paper. Correspondence and requests for materials should be addressed to E.H. (hassanpe@oregonstate.edu)

3. Chapter 3: Agrivoltaics Role in the Water- Food- Energy Nexus

Elnaz Hassanpour Adeh[1], M. Abou Najm[2], Chad W. Higgins[1*]

[1] Department of Biological and Ecological Engineering, Oregon State University, Corvallis, USA
[2] Department of Civil and Environmental Engineering, American University of Beirut, Beirut, Lebanon
*Corresponding author, Email: chad.higgins@oregonstate.edu, Tel: 541-737-2286

3.1 Abstract

Water, food and energy are essential elements for human life and they all are interconnected. Rising global population, rapid urbanization and economic growth, they all need water, food and energy. Efficient resource management is therefore of great importance. However, these resources are distressed and extending available resources can benefit the world. In this paper, we present an example of Agrivoltaics which can extend our available resources and reduce the completion for land while producing clean energy and food and reducing water demand. We used integrated model of solar panel by changing the shade percentage on most productive crops in Oregon potato and barely. AquaCrop was applied to estimate the effect of shading percentages on crops biomass and water use efficiency.

3.2 Keywords

Agrivoltaics, Land competition, Water Food Energy Nexus, Water Efficiency, Crop Productivity, Shade

3.3 INTRODUCTION

Humans need water, food and energy. Cities were built near water, food or energy resources to survive. It wasn't as complicated as today's situation where fossil fuels are diminishing, making Green House Gas (GHG) emissions, running out of ground water supplies, which ultimately reduces food for life. Clean affordable energy, adequate food and improved nutrition for all. Clean water for people and ecosystem, protected and sustained environment, all these challenges are tightened to each other. Harvesting

solar excess with solar panels produces energy while the panel shade reduces water demand and less stressed plants. On the other hand, plant transpiration cools the microclimate which leads to higher solar power efficiency.

Simulation studies show shade under panels changed mean soil temperature, evapotranspiration and soil water balance which lead to better condition for plant production compared to full sun (Amaducci et al., 2018). Combination of photovoltaics and agriculture on the same field increases the total leaf area per plant, the size of leaves in the shade and also land equivalent productivity by 35-73% (Marrou et al., 2013) (Dupraz et al., 2011). Experimental study by hassanpour et al. confirms the simulation by resulting in 90% more dry biomass and 328% more water efficient for grazing grasses(Hassanpour Adeh et al., 2017). In addition, with the projected future climate change, generating yield predictions and for improving water use, the result may be of interest to climatologists, agriculturists and policy makers. Under water constraint environment (Oregon summer), there have been needs to evaluate the possibilities of maximizing yield and biomass through irrigation. This can be achieved through the use of a validated water productivity model such as AquaCrop. The objective was to use AquaCrop model for simulating crop yield over three shade level with same planting dates and water availability conditions and to evaluate the performance of the model in evaluating water use efficiency in Oregon. Potato and barely are the major crops in Willamette valley, Oregon. Potato and barely account over 50% and 23% of the crop production of Willamette valley respectively ("facts_and_figures.pdf," n.d.). AquaCrop model is developed by Food and Agricultural Organization (FAO) to evaluate the water use efficiency and water productivity which best fits the location. The model deals with yield response to water. Water, energy, and food are highly inter-connected and understanding the connection and quantifying the variables can help clarifying this complex system (Mohtar & Daher, 2012). In many regions, land under cultivation could simultaneously be used for renewable energy production. Multi-use of land for agriculture and energy purposes is becoming common, such as wind turbines constructed on grazing land; biogas plants used for treating animal manure with nutrients recycled to the land. Leasing farm land to renewable energy developers, such

as solar, can be a source of additional income. Solar farms may also enhance the agricultural value of land, like more productive grazing pasture. This concept actively encourages multi-purpose land use, through continued agricultural activity or agri-environmental measures that support biodiversity, yielding both economic and ecological benefits (BRE, 2014)(Ferroukhi et al., 2015).

It is commonly proposed in planning applications for solar farms that the land between and underneath the rows of PV modules be available for grazing small livestock. Sheep and free-ranging poultry already have been successfully employed to manage grassland in solar farms while demonstrating dual-purpose land use (Hernandez 2014). Special structures are being deployed involving rows of PV panels mounted above ground and arranged at certain intervals to allow enough sunlight for photosynthesis and space for agricultural machinery to be used. Several "solar sharing" plants have been developed. In Corvallis, Oregon, the 1.5 MW Solar Sharing Project on a 6 acre farm mounted 2 meters from the ground. Under the panels native grasses are grown[4] (Hassanpour Adeh et al., 2017).

3.4 MATERIAL AND METHODS

Site description

Potato and barley selected as the major crops grown in Oregon. Daily evapotranspiration, temperature, precipitation, solar radiation, humidity and wind speed data for the AquaCrop model used from Hermiston and Madras stations, Agrimet ("AgriMet Pacific Northwest Region | Bureau of Reclamation," n.d.). Precipitation in Willamette river ranges from 900 mm to 2000 mm annually ("Land-Based Station Data | National Centers for Environmental Information (NCEI) formerly known as National Climatic Data Center (NCDC)," n.d.). Daily reference evapotranspiration values were calculated using FAO-Penman- Monteith equation based on full data sets (daily mean wind speed, temperature, relative humidity and reference evapotranspiration) as described in Allen et al. (1998)(Allen et al., 1998). The maximum and minimum temperatures at the two sites during the growing periods was different. Soil physical characteristics such as bulk density (1.33 gr/cm^3), texture

(silt loam), depth (2.3 m) were determined from Web Soil Survey (websoilsurvey.sc.egov.usda.gov).

Field layout, cultural practice and measurements

The planting and harvesting time shown in table 3.1. The treatments were planting time and water (rainfed and/or rain- fed + irrigation). Two planting dates based on the local farmer's practice were used: September (early planting under rain- fed condition), May (normal planting under irrigation condition early planting under rain- fed condition).

Table 3. 1 Planting/ harvesting time

crops	Planting	harvesting
Barley	01/09/2003	30/04/2017
potato	01/05/2003	30/10/2017

All crop management techniques were carried out following regional recommendations. For example, the barley cultivar was sown by broadcasting.

Crop parameters and measurements

The days from sowing to emergence, maximum canopy cover, start of senescence, and physiological maturity, as well as maximum rooting depth were selected from USDA online information. With the given temperature data sets the model estimated the degree days for each crop development. The conventional destructive technique of root length measurement (washed out of soil samples from roots) was used in the model. Canopy cover was estimated from leaf area index based on Ritchie type of equation (Belmans et al., 1983) (Ritchie, 1972). In the AquaCrop model the evapotranspiration ET_o rate from a alfalfa is selected as a reference surface and is an index for the evaporating power of the atmosphere. Soil evaporation (E) is calculated by multiplying ETo with the soil evaporation coefficient (Ke) and by considering the effect of water stress:

$E = (Kr^* Ke)^*ET_o$

where Kr is the evaporation reduction coefficient which becomes smaller than 1, and as such reduces soil evaporation, when insufficient water is available in the soil to respond to the evaporative demand of the atmosphere. The soil evaporation coefficient Ke is proportional to the fraction of the soil surface not covered by canopy (1-CC). The proportional factor is the maximum soil evaporation coefficient (Kex) which integrates the effects of characteristics that distinguish soil evaporation from the evapotranspiration from the grass reference surface.

When the surface is wet, soil evaporation is calculated by multiplying the reference evapotranspiration (ETo) with the soil evaporation coefficient. The soil evaporation coefficient, Ke, considers the characteristics of the soil surface and the fraction of the soil not covered by the canopy:

$Ke=(1-CC^*)Ke_x$

where (1-CC*) adjusted fraction of the non-covered soil surface and Kex is the maximum soil evaporation coefficient for fully wet and not shaded soil surface. In our model we changed the Ke_x which is a shade factor to three levels of 0 %, 25 % and 50 %.

3.5 RESULTS

Plants are developmentally and physiologically designed to reduce water use (WU) under water stress. Water use efficiency (WUE) is yield per available water or water applied (by evapotranspiration) which the term is generally is used by farmers for irrigation but water productivity (WP) is defined as yield per water consumed (by transpiration) which the term is used by agronomists (van Halsema & Vincent, 2012). Here in this paper we are interested in water use efficiency which is often considered an important determinant of yield under stress. It is found that if water is the limiting factor of crop growth, any increase in WUE will lead to increase the yield. In this simulation drought stress on crops is mitigated by introducing the shade. Our results show there is no difference in yield when shade is applied but the amount of water

needed for irrigation is reduced. Figure 3.1 shows the amount of water is needed to irrigate barely at three shade levels. Additionally, if we increase the shade by 50% no irrigated water is needed. Figure 3.2 shows the irrigated water for potato from 2003 to 2016.

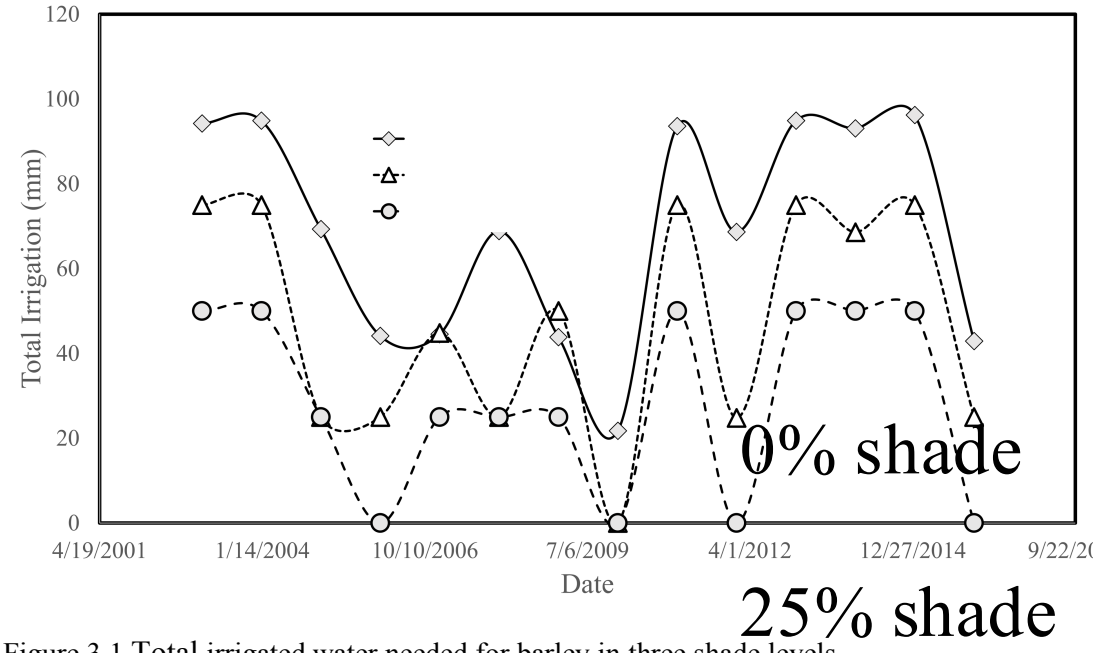

Figure 3.1 Total irrigated water needed for barley in three shade levels

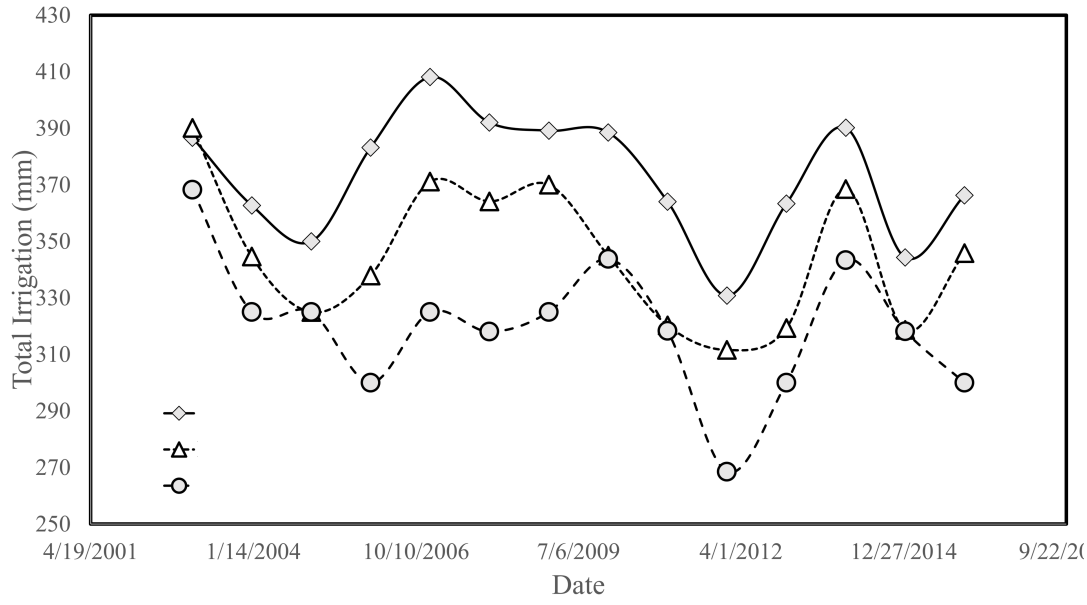

Figure 3.2 Total irrigated water needed for potato in three shade levels

The biomass results showed no gain or loss occurs in different shade levels but there is a difference in the amount of irrigated water. It means we can have the same yield by applying the shade and saving water. 50% , 25% and 0% shade slightly improved the water use efficiency in all years. But this has not resulted in significantly higher biomass. This indicates barley and potato has shown a tendency to respond positively to increasing the shade levels.

3.6 DISCUSSION

The model simulated the water use efficiency for three shade levels for barley and potato. Total irrigated water needed for barely even reaches to zero at some years, which means shade can afford the available water for optimum yield. The total water needed for potato is higher than barley but still the amount of water for optimal grow decreases when shade increases. The implication is that in semi-arid environment and with no restriction of arable land like the case of eastern Oregon, shade may save water and improve barley and potato water use efficiency. By running the model under

0% shade

25% shade

different shade levels, it is possible to optimize the barley and potato water use efficiency. The essence of optimal water use efficiency may differ from place to place but in our case optimal planting is the planting date which allows the crop to use maximum natural rainwater leading to a relatively proper growing period for relatively maximum biomass and water use efficiencies.

Furthermore, using the model it is possible to explore biomass yield per unit of water supplied/used. In this simulation, barley and potato under shade showed less water is needed for irrigation. The model can be improved by using field calibration and validation. Assuming that water is scarce (eastern Oregon) the model indicated the possibilities of obtaining relatively same biomass if shade applies instead of more irrigation.

3.7 Reference

AgriMet Pacific Northwest Region | Bureau of Reclamation. (n.d.). Retrieved June 27, 2018, from https://www.usbr.gov/pn/agrimet/

Allen, R. G., Pereira, L. S., Raes, D., & Smith, M. (1998). FAO Irrigation and drainage paper No. 56. *Rome: Food and Agriculture Organization of the United Nations*, *56*(97), e156.

Amaducci, S., Yin, X., & Colauzzi, M. (2018). Agrivoltaic systems to optimise land use for electric energy production. *Applied Energy*, *220*, 545–561. https://doi.org/10.1016/j.apenergy.2018.03.081

Dupraz, C., Marrou, H., Talbot, G., Dufour, L., Nogier, A., & Ferard, Y. (2011). Combining solar photovoltaic panels and food crops for optimising land use: towards new agrivoltaic schemes. *Renewable Energy*, *36*(10), 2725–2732.

facts_and_figures.pdf. (n.d.). Retrieved from https://www.nass.usda.gov/Statistics_by_State/Oregon/Publications/facts_and_figures/facts_and_figures.pdf

Ferroukhi, R., Nagpal, D., Lopez-Peña, A., Hodges, T., Mohtar, R. H., Daher, B., et al. (2015). Renewable energy in the water, energy & food nexus. *IRENA, January*.

van Halsema, G. E., & Vincent, L. (2012). Efficiency and productivity terms for

water management: A matter of contextual relativism versus general absolutism. *Agricultural Water Management*, *108*, 9–15.

Hernandez, Rebecca R., et al. "Environmental impacts of utility-scale solar energy." Renewable and sustainable energy reviews 29 (2014): 766-779. https://doi.org/10.1016/j.agwat.2011.05.016

Land-Based Station Data | National Centers for Environmental Information (NCEI) formerly known as National Climatic Data Center (NCDC). (n.d.). Retrieved July 17, 2018, from https://www.ncdc.noaa.gov/data-access/land-based-station-data

Marrou, H., Wéry, J., Dufour, L., & Dupraz, C. (2013). Productivity and radiation use efficiency of lettuces grown in the partial shade of photovoltaic panels. *European Journal of Agronomy*, *44*, 54–66.

Mohtar, R. H., & Daher, B. (2012). Water, energy, and food: The ultimate nexus. *Encyclopedia of Agricultural, Food, and Biological Engineering. CRC Press, Taylor and Francis Group*.

Selker, J. S., Hassanpour Adeh, E., & Higgins, C. W. (2017). Remarkable solar panels Influence on soil moisture, micrometeorology and water-use efficiency-database.

4. Chapter 4: An Investigation on indirect wind turbine water demand in evapotranspiration form: A case study for Fowler Ridge windfarm, Indiana

Elnaz Hassanpour Adeh[1], Marc Calaf[2], Chad Higgins[1*]

[1] Department of Biological and Ecological Engineering, Oregon State University,
[2] Department of Mechanical Engineering, University of Utah, UT, USA
* Corresponding author, Email: chad.higgins@oregonstate.edu, Address: 116 Gilmore Hall, 124 SW 26th St, Corvallis, Oregon 97331, US, Tel: +15417372286

4.1 Abstract

As a vital component of renewable energy systems for a sustainable future, wind energy is among the fastest growing sources worldwide. More than 26% of wind farms have some irrigated agriculture within their footprint and there is no specific research that addresses the long-term effects of co-located wind turbines on indirect water demand

increases of irrigated agriculture due to potential changes in evapotranspiration processes. A methodology was developed in this paper for spatial and temporal evapotranspiration analysis of irrigated fields using remotely sensed input data from satellite platforms. The proposed methodology includes an algorithm development for automated processing and analysis of Landsat data and using the METRIC method in batch-mode to investigate the long-term effects of wind turbines on evapotranspiration on the wind farms. The developed framework is generic and can be used for any location with available input data. For this paper Fowler Ridge wind farm in Indiana, US was analyzed, as a case study where approximately 300 wind turbines were installed in this wind farm in 2008 and 2009. The satellite demand evapotranspiration estates increase approximately 15% within the footprint of wind turbines for the selected snap shot dates. This increase is even comparable with other high water demanding energy sources (e.g., nuclear energy).

4.2 Keywords

Wind Energy, Evapotranspiration, Wind Footprint, Irrigated Agriculture, METRIC

4.3 Introduction

Wind turbines have been promoted as an energy source that does not require a large expenditure of water. However, recent simulation results indicate that wind turbines increase evaporation rates from the nearby irrigated lands (Porté-Agel et al., 2011). The additional water demand due to the wind turbines, must be met through increased irrigation to maintain full production. Evaporation has been used previously as a metric for water consumption, for example, in hydropower production (R. Saidur, 2011)(Higgins et al., 2015).

Since wind turbines can alter the humidity, temperature and wind velocity profiles near the surface, they can significantly change the evaporation amounts from land surface and numerical studies support this idea. A study by (Calaf et al., 2011) shows that the evaporation may increase by 15% in windfarms compared to bare lands .Studies parameterized the effects of the wind turbines over the atmospheric flow (Fitch et al., 2013) and explored the interaction of wind turbines with intensive agriculture

(Rajewski et al., 2013) (Smith et al., 2013). The conceptual studies for environmental impacts of wind turbine installations already consider construction aspects and some additional factors, e.g., esthetics, noise, and danger to migratory bird populations (Pookpunt & Ongsakul, 2013)(Dai et al., 2015).

In this study, we address the interactive effects of wind turbines on their local environment, water resources usage and the changes in water demand estimation through evapotranspiration. The Fowler Ridge wind farm is located in Indiana, US, where approximately, 300 wind turbines were installed in two phases from April 2008 to January 2010 ("The Fowler Ridge Wind Farm Project, USA," n.d.) . The goal of this research was to monitor the evapotranspiration variations before and after wind turbine installations using satellite and weather data. Mapping evapotranspiration with Internalized Calibration (METRIC) was used on Landsat data spanning long intervals for the wind farm (Allen et al., 2007). The evapotranspiration comparisons were performed between in and out of wind turbine footprints, for which eclipse shapes were assumed. Since the exact footprint characteristics are still unknown in the literature, parametric studies were performed on input area of footprint, distance from the wind turbine and the angle with respect to wind directions. The parametric sweep studies resulted in the possible range of evapotranspiration difference between the in and out area, using statistical approaches (e.g., t-test).

The results of the case study analysis are significant and indicate large indirect water usage by wind turbines that are collocated with windfarms. The results on Fowler Ridge wind farm showed an increase of approximately 10% for compared evapotranspiration between inside and outside the wind turbine footprints.

4.4 Materials and methods

An automated algorithm was developed to handle the data analysis for multiple snap shots from a certain wind farm. The developed code calculates the ET, using a METRIC method (as briefly discussed in the next section) and performs the comparisons based on variable footprint parameters. In addition to required images, the weather information are needed to obtain the minimum and maximum temperatures, average daily wind speeds, average daily relative humidity, etc. as described briefly hereafter.

Input data

The main input data for a generic wind farm includes: satellite, weather, wind farm geographical boundaries and wind turbine data. The satellite data are obtained from Landsat missions USGS website ("EarthExplorer," n.d.). The Thematic Mapper (TM) bands 1-5 and 7 for Landsat 7, can provide visible and near infrared data (Allen et al., 2007), with 30×30 m^2 pixel size. The daily weather data were obtained from closest weather station (less than 50 km), Lafayette, Purdue University Airport (KLAF), with latitude of 40.25° N and longitude of -86.56°W and elevation of 596 ft. for Fowler Ridge wind farm. Additionally, the wind turbine locations is derived from Google Earth ("The Fowler Ridge Wind Farm Project, USA," n.d.). Wind farm boundaries is drawn 1200 meters from the border turbines assuming 15 times of rotor diameter which are 81 meters (Meyers & Meneveau, 2012). We choose cloud free days on growing season from June—August. In total, various scenes prior to and after wind turbine installations were considered to monitor the compared ET inside and outside the wind turbine footprints.

Mapping Evapotranspiration with Internalized Calibration (METRIC)

The methodology of this research relies on the evapotranspiration calculations based on METRIC method (Allen et al., 2007). The input data for these calculations are provided by satellite (Landsat) and weather data. The evapotranspiration can be obtained from the residual energy as

$$\lambda ET = R_n - G - H \qquad \text{Equation (1)}$$

Where λET is the latent heat flux (W/m^2) calculated for each pixel of the image at the certain time of taking the image by satellite. Also, Rn, G and H are the net radiation flux at the surface (W/m^2), soil heat flux (W/m^2) and sensible heat flux to the air (W/m^2), respectively. The net surface radiation is obtained taking the incoming shortwave/longwave and outgoing longwave radiant fluxes. The surface albedo and surface thermal emissivity play important roles in calibrating the actual incoming and outgoing values as

$$R_n = (1-\alpha)R_{s\downarrow} + R_{L\downarrow} - R_{L\uparrow} - (1-\varepsilon_0)R_{L\downarrow} \quad \text{Equation (2)}$$

Where S and L stand for shortwave and longwave, respectively. α and ε_0 are also surface albedo and surface thermal emissivity, respectively. Table 4.1 shows the calculation procedures for different parameters in Eq. (1) for evapotranspiration calculation.

Table 4.1: Data preparation and calculations methods for evapotranspiration calculation using METRIC methodology

Parameter	**Method of calculation**	**Input data**
Surface Albedo (α)	Weighted average based on spectral radiance	Satellite image information on spectral radiance for each satellite band
Incoming shortwave radiation ($R_{s\downarrow}$)	Direct and difuse solar radiation flux	Solar constant, the solar incidence angle, a relative earth-sun distance and atmospheric transmissivity
Incoming longwave radiation ($R_{L\downarrow}$)	Modified Stefan-Boltzmann equation	Atmospheric transmissivity and a selected surface reference temperature
Outgoing longwave radiation ($R_{L\uparrow}$)	Stefan-Boltzmann equation	Calculated surface emissivity and surface temperature
Surface temperature (T)	Plank equation	Satellite image information on thermal radiance.
Surface emissivity (ε_0)	Empirical function	Vegetation index
Soil heat flux (G)	Empirical function	vegetation indices, surface temperature, and surface albedo

Sensible heat flux (H)	Iterative procedure	Wind speed observations, estimated surface roughness, and surface to air temperature differences

The equivalent amount of instantaneous ET (mm/hr) is obtained by dividing by the latent heat of vaporization (λ). The details of the METRIC method are omitted for the sake of brevity and can be found in (Allen et al., 2007).

Developed algorithm for ET calculation and data analysis in batch mode

The initial part of the developed algorithm acquires the Landsat 7 data as input and obtains evapotranspiration (ET) as a result. The results are then post-processed to calculate the variations of ET comparisons, before and after wind turbine installations. Figure 4.1 shows the general algorithm, developed for the first part, i.e., ET calculation in each pixel.

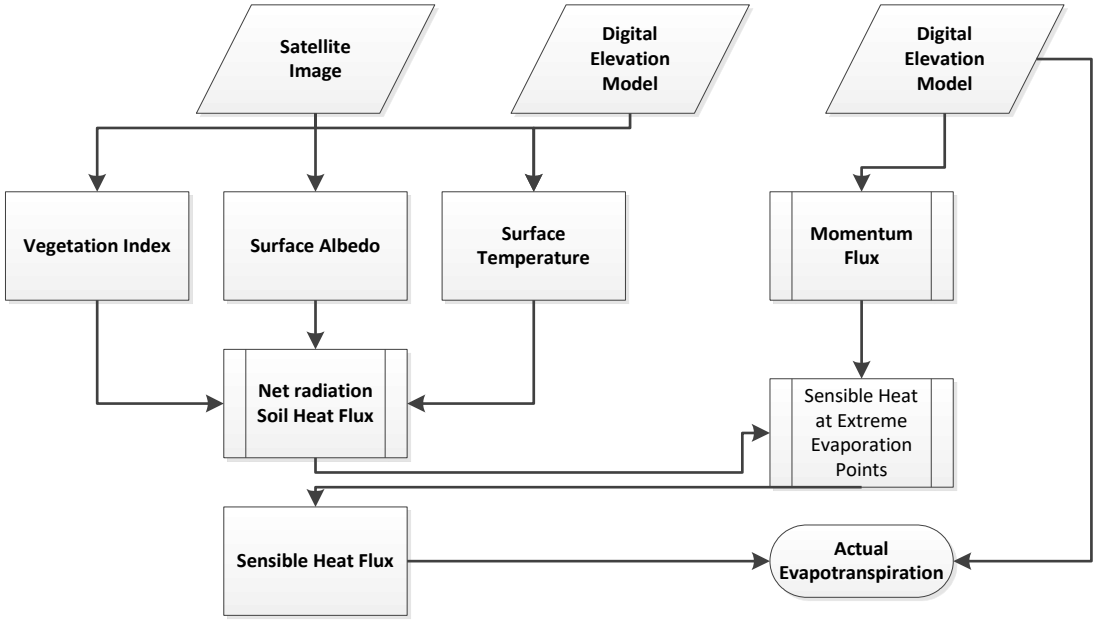

Figure 4.1 Developed algorithm for METRIC-based ET calculations and post-processing

As the first part of the developed methodology, the presented algorithm in Figure 4.1 is quite similar to existing SEBAL algorithm and is not discussed further in this paper for brevity, see e.g., developed in ERDAS IMAGINE . The main point of the developed algorithm is an automatic cold and hot pixel selection for boundary conditions in

sensible heat flux calculation. The general conditions for these selections that were programmed, included: (a) cold pixel: well-watered and full vegetated area (LAI>4 and albedo>0.22) with zero sensible heat flux and assumption of 1.05ETr for evapotranspiration (similar to Idaho); (b) hot pixel: dry and bare agricultural field (LAI<0.4) with no evapotranspiration. It's noted that the selection algorithm for hot pixel is trial and error because authors needed to manually recheck if the selected pixel is not located on asphalt or bare field. Briefly, the calculations are performed with an arbitrary hot pixel selection, and the surface temperature is calculated. The actual hot pixel is the selected based on the maximum temperature that can happen in a dry and bare agriculture are, which is handled manually.

Footprints

The second part of the automatic methodology in this paper is statistical comparison of calculated ET inside and outside of the wind turbine footprints. However, according to authors' knowledge, there is no physics based model that describes the footprint of impacted land area downwind of wind turbines. Therefore, in this study an optimization approach was taken that interrogates many possible footprint areas, aspect ratios and positions, for each potential footprint, to maximize the differences in and out of the footprints. All investigations in this paper are based on the following main assumptions:

- An elliptical form (Figure 4.2) was assumed, parametrized by the axes of the eclipse, the placement of the eclipse downwind and the angle of the eclipse, determined by the wind direction;
- It was assumed that all wind turbines have similar footprints for a certain scene and;
- The wind farm boundaries were obtained assuming a 50-m buffer from the peripheral wind turbines.

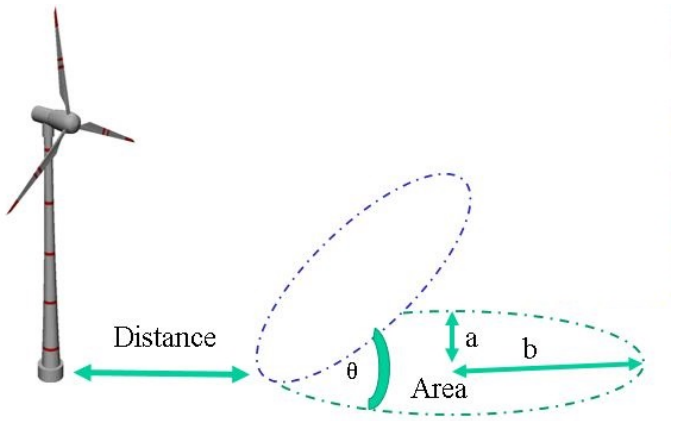

Figure 4.2 The potential variables for eclipse shape footprints. The inclination angle is considered with respect to the wind direction.

The full range of parameters explored is presented in Table 4.2 and the change in evapotranspiration was calculated for each parameter set. According to Table 4.2, the resulted footprints may (or may not) overlap. Because the only final use of this will be comparing the ET data inside and outside the footprints, having overlaps will not cause any issues with the method.

A typical turbine spacing of eight rotor diameters is used, with one turbine per grid cell. The decision on parameter range for the studies was based on available references and therefore, it can be enhanced. First, the distance was assumed between 8 D which is a typical turbine spacing of eight rotor diameters is used, with one turbine per grid cell. (Fitch et al., 2013). This results in approximately 240 meters, as noted in Table 4.2. The Angle was also determined from the 75% confidence interval based on average decade data from [REF to cli-Mate Database: https://mrcc.illinois.edu/CLIMATE/Hourly/WindRose.jsp]. Figure 4.3 shows the wind rose.

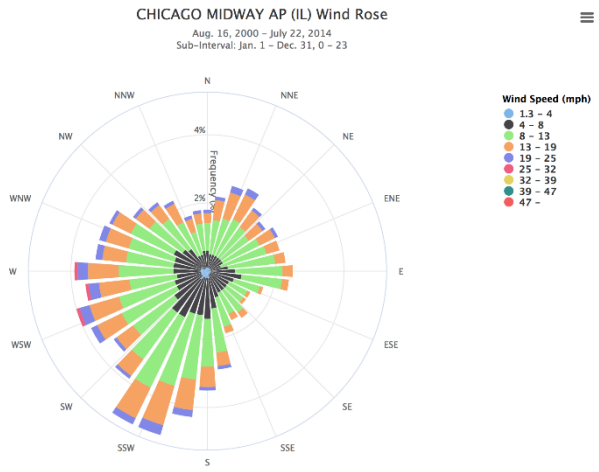

Figure 4.3: The wind rose diagram for January, 1, 2000 to December, 31, 2014 for Lafayette, Purdue University Airport (KLAF) weather station

The 75% confidence interval is then derived based on the directions from Figure 4.3, as 0º (East) to 270º (South). It's noted that assuming some parameter combination not only could result in overlap, but also could result in footprints located outside of the windfarm area.

Table 4.2 Parameter variability for footprints. Note: each pixel area is 9×10^{-4} km^2

Parameter	**Minimum**	**Maximum**
Distance	240 m	600 m
Area	0.2 Km^2	2.0 Km^2
Aspect ratio	1	5
Angle	0	270º

The whole assumed set of parameters were studied for each scene at each date and the results of inside to outside evapotranspiration ratios were stored as vectors. The total number of analyses for each scene was 2250. The approach in this research included development of an algorithm for automatic pixel selections as a function of considered variable in Figure 4. 2 (eclipse radius, angle of inclination and distance to wind turbine). Briefly, the ET of pixels inside the footprint were compared the outside ones. Figure 4.4 shows the algorithm flowchart for the comparison approach.

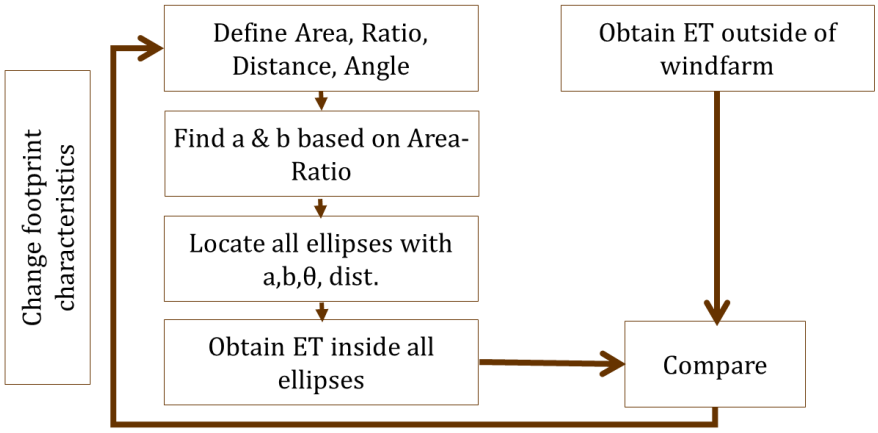

Figure 4.4 Developed algorithm for optimization process of obtaining the best eclipse footprints

The Case study: Fowler Ridge wind farm

The Fowler Ridge wind farm is one of the largest onshore wind farms in the world, located in Benton county, Indiana, US. It covers approximately 200 km^2 and production capacity of 750MV with 350 wind turbines. Fowler wind farm was installed with phase I in April 2008. Figure 4.5 shows the location of this wind farm within the US and the satellite image bounding box.

(a)

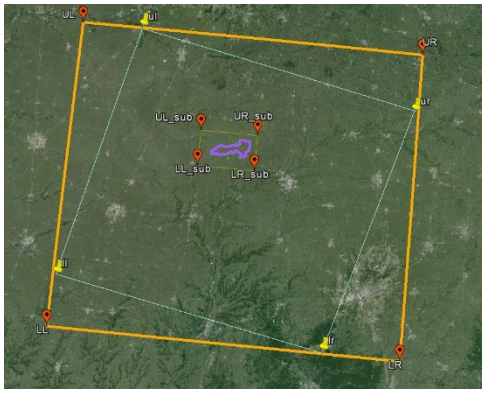

(b)

Figure 4.5 Fowler Ridge wind farm: (a) satellite bounding box and (b) the coordinates of UL (Upper Left), UR (Upper Right), LL (Lower Left) and LR (Lower Right) and their sub-regions are mentioned in Table 4.2

Figure 4.5(a) shows the approximate location of the wind farm in the US and Figure 4.5(b) represents the satellite image box (in yellow), bounding box (in white and wind

farm actual boundaries (in violet) assuming a 50 m buffer from the peripheral wind turbines. Table 4.3 and 4 show the coordinate of bounding box for the studies wind farm. These coordinates along with other required led values (e.g. wind turbine coordinates) were taken using Google Earth software ("EarthExplorer," n.d.).

Table 4.3 Satellite image coordinates provided by US Geological Survey

Point	Latitude (degrees)	Longitude (degrees)
UL	41.29721	-88.73307
UR	41.30421	-85.8198
LL	39.35478	-88.68407
LR	39.36131	-85.85317

Table 4.4: Coordinates of bounding box for Fowler Ridge wind farm

Point	Latitude (degrees)	Longitude (degrees)
UL	40.67850311684456	-87.62726964181525
UR	40.68010442683556	-87.15395202194598
LL	40.45329362346066	-87.62517054043886
LR	40.45488232583604	-87.15343679687264

We used the boundary buffer around the wind farm to capture all possible wind effect on surrounding farm.

4.5 Results

Using the METRIC algorithm, presented in Table 4.1, ET was calculated on the bounding box for dates of interest. The required ET calculation steps include calculating surface albedo, incoming shortwave radiation, outgoing longwave radiation, incoming longwave radiation and solving the energy balance equation. Sample step by step results will be shown for one date in this section.

Dates of interest

The goal is to compare the ET inside the wind turbine footprint and outside the area before and after installation for the growing season. Wind turbine construction April 2008 – January 2010, therefore scenes were taken before and after this time range (see Table 4.5). The average 24-hour wind speed is also mentioned in the table for comparison purposes. Selected dates are the most cloud free images from satellite which are taken every 16 days..

Table 4.5: Dates for evapotranspiration data analysis on Fowler Ridge wind farm and average wind speed values

No.	Before construction (wind speed (m/s))	After construction (wind speed (m/s))
1	08/16/2000, (3.56)	08/28/2010, (2.53)
2	07/21/2002, (3.17)	06/28/2011, (3.85)
3	07/29/2005, (2.20)	08/01/2012, (2.27)
4	08/06/2008, (3.09)	07/22/2014, (3.11)

Sample step by step results ET calculations

According to Eq. 1, ET can be obtained after net radiation, sensible heat and soil heat flux are found. In this section, the required steps towards ET calculation for a specific case are sown. The chosen date for sample outputs was before installation on Aug, 16, 2000.

The surface albedo and its histogram were obtained from top-of-atmosphere albedo correction using average portion of the incoming solar radiation and transmissivity of both direct solar beam radiation and diffuse (scattered) radiation to the surface. The top-of-atmosphere albedo was itself calculated using the weighted approach over reflectivity values that had been found from spectral radiance. The spectral radiance is directly related to Digital Number (DN) of each pixel. Figure 4.6 (a) shows the surface albedo obtained for the abovementioned date for Fowler Ridge wind farm. According to Figure 4.6 (b) the calculated values fall mostly between 0.15 and 0.30.

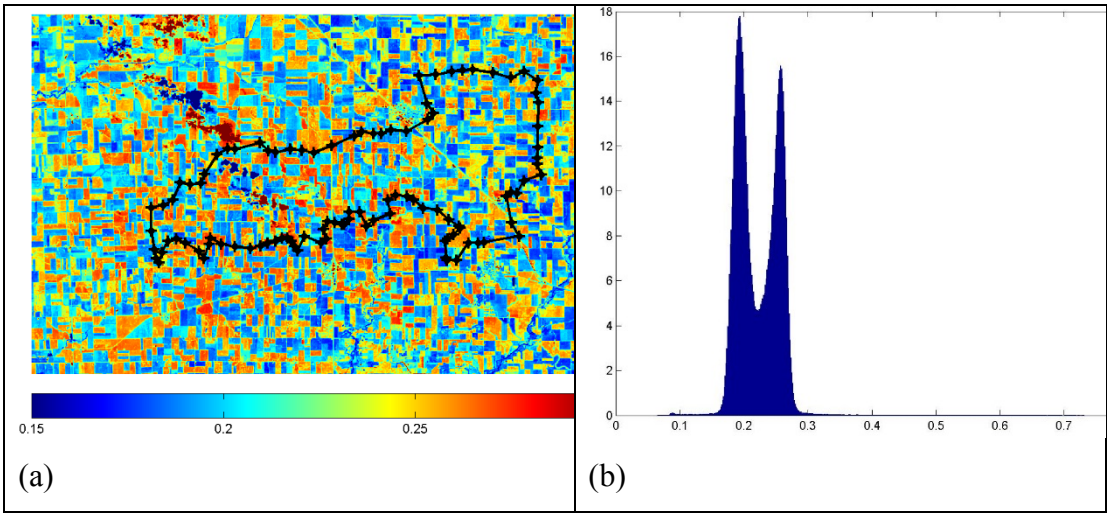

Figure 4.6 Calculated surface albedo for 08/16/2000 in Fowler Ridge wind farm: (a) image and (b) histogram. The windfarm boundaries are shown in black

The surface temperature is then estimated using emissivity representing surface behavior for thermal emission, which itself is expressed as a function of Normalized Difference Vegetation Index (NDVI) and surface albedo. Figure 4.7 shows the surface temperature for the bounding box, assumed for Fowler Ridge wind farm.

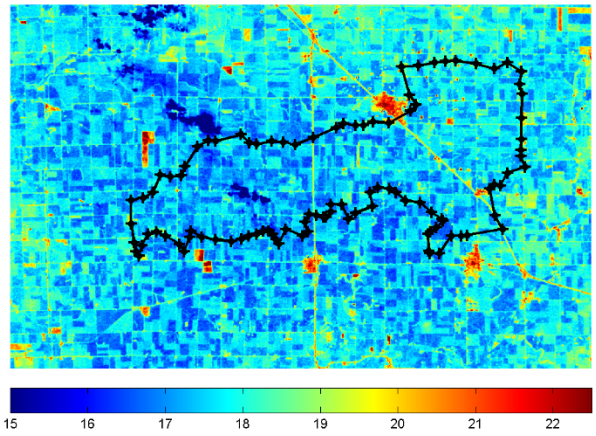

Figure 4.7 Calculated surface temperature (^{o}C) for 08/16/2000 in Fowler Ridge wind farm. The windfarm boundaries are shown in black

The sensible heat can be estimated using an iterative procedure where the boundary conditions in cold and hot pixels can satisfy the energy balance. In fact, for solving the energy balance equation using the METRIC method, two boundary conditions are required. These boundary equations are applied using ‘cold’ and ‘hot’ pixels. Choosing

these pixels performed manually, since many qualitative conditions need to be satisfied, including (a) a dry bare agricultural field with maximum surface temperature and zero ET for hot pixel and (b) a wet, well-irrigated crop surface having full ground cover by vegetation as cold pixel. For detail information on choosing these pixels and applying the boundary conditions, see e.g., Appendix 7 of METRIC manual. Figure 4.8shows the sensible heat flux obtained for the current problem.

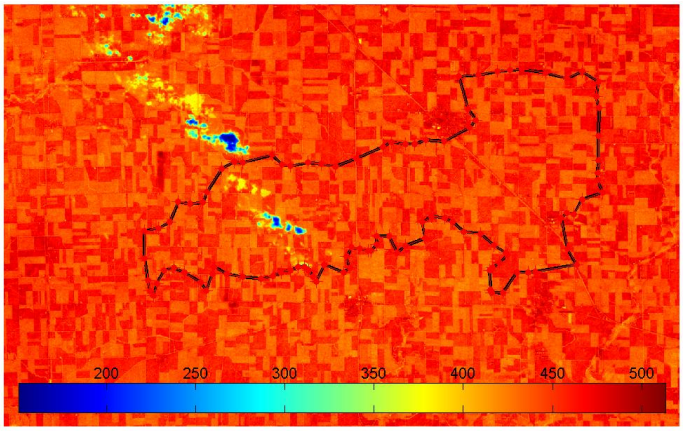

Figure 4.8 Calculated sensible heat flux (W/m^2) for 08/16/2000 in Fowler Ridge wind farm. The windfarm boundaries are shown in black

Figure 4.9 also shows the soil heat flux, which can be obtained from the surface temperature, NDVI and surface albedo.

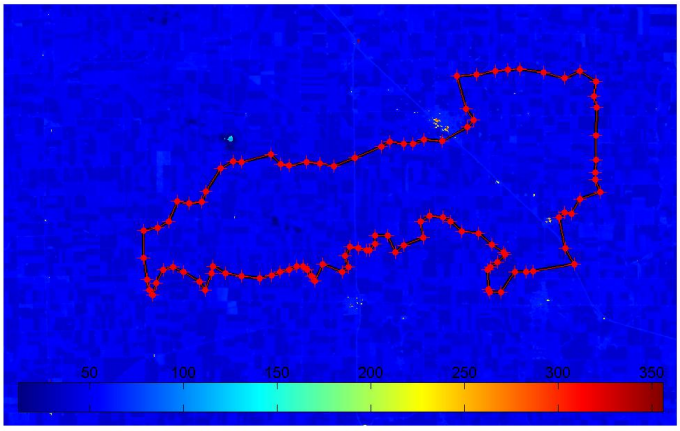

Figure 4.9 Calculated soil heat flux (W/m^2) for 08/16/2000 in Fowler Ridge wind farm. The windfarm boundaries are shown in black

The last part of the energy balance equation is the net radiation at surface which is actually an algebraic summation over incoming shortwave incoming/outgoing

longwave radiation, with the effects of surface albedo and emissivity considered. Figure 4.10 shows the net radiation. The evapotranspiration is finally calculated using Eq. 1, for each pixel.

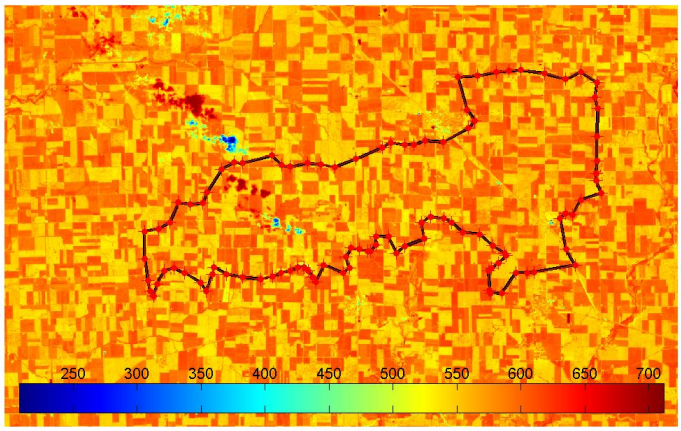

Figure 4.10 Calculated net radiation (W/m^2) for 08/16/2000 in Fowler Ridge wind farm. The windfarm boundaries are shown in black

4.6 Discussion

The developed automated algorithm was applied for various dates from Table 4.5. For each scene all parameters in Table 4.2 were analyzed for average ET inside and outside of the farm. The specific footprints was calculated and the ratio was stored in a matrix, therefore:

$$\text{ratio} = \frac{\text{ET}_{\text{in}}}{\text{ET}_{\text{out}}} \qquad \text{Equation (3)}$$

where ET_{in} and ET_{out} re the average ET inside and outside of the footprints. Figure 4.11 shows the resulted footprints from one case study with distance, area, aspect ratio and wind direction of 30 m, 0.222 km^2, 2 and 30^o, respectively. The footprints may easily have overlaps with larger distance or areas, however, the only usage of this setting is comparing the calculated ET inside and outside of the footprints, therefore, there will be no issues with having overlaps.

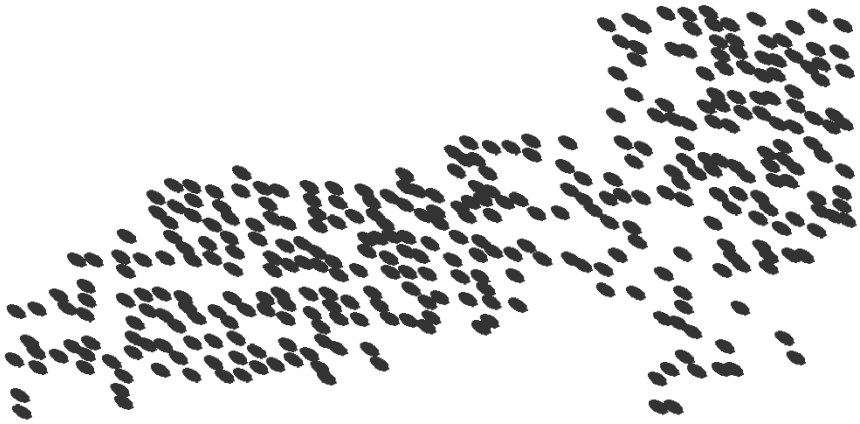

Figure 4.11 The footprints automatically resulted from a sample case study in the parametric sweep analysis

Finally, for each scene, which corresponds to a certain date, a vector of ratios is obtained from Eq. (3). Figure 4.12 shows the resulted analysis (as box plots) for these ratios (on vertical axis) versus different dates and the dashed line approximately shows the installation time.

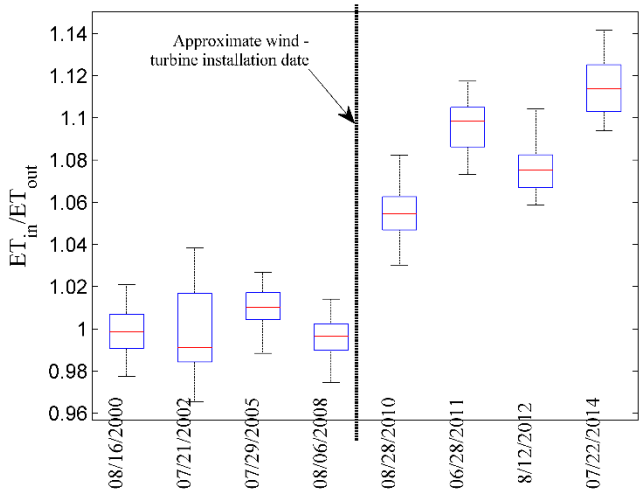

Figure 4.12 Variation of ET_{in}/ET_{out} over time. The dashed line shows the approximate wind turbines installation time

The variability of resulted ratios are shown in box plot forms where median, 25-75% confidence intervals and min/max values are presented. The thick line in the plot represents the first phase installation approximate date. The main finding from Figure

4.12 is the increasing trends of ET ratios after the wind turbines installations in 2008. A comparison between 2000-2005 and 2012-2014 shows an approximate of 10\% increase in the average ratio which is definitely related to the effects of collocated wind turbines after 2008. Additionally, there doesn't seem to be a significant increase in ET ratios until 2010, which might be partially related to the fact that the installations wind turbine installations were completed in 2009.

4.7 Conclusion

Surface fluxes measured upwind and downwind of a line of turbines give evidence of conditional crop microclimate modification by individual wind turbines. Our results show that the turbines did increase the ET after wind turbine installation for Fowler Ridge Farm. The results showed an approximate increase of 10% in ET inside the possible footprints after wind turbine installations. Concurrent differences in ET changes are significant at a discussed wind turbine footprint. It's noted that our results are for a specific location and climate, these results may change on different climate.

The cloud free images were used that are necessary for the satellite measurements. This resulted in limited number of snap shots and total available data. Future studies would require several measurement systems at multiple locations of multiple turbine to ascertain what climatological impacts are possible from large wind farms on agricultural water demand. Additionally, the determination of footprints for the wind farm is out of the scope of this paper, however, a potential procedure of an average configuration for a certain windfarm may be resulted from an optimization method, where ET_{in}/ET_{out} is maximized.

4.8 References

Al- Sabounchi, A. M. (1998). Effect of ambient temperature on the demanded energy of solar cells at different inclinations. *Renewable Energy*, *14*(1), 149–155. https://doi.org/10.1016/S0960-1481(98)00061-5

Allen, R. G., Tasumi, M., & Trezza, R. (2007). Satellite-based energy balance for mapping evapotranspiration with internalized calibration (METRIC)—Model. *Journal of Irrigation and Drainage Engineering*, *133*(4), 380–394.

Appelbaum, J., & Bany, J. (1979). Shadow effect of adjacent solar collectors in large

scale systems. *Solar Energy*, *23*(6), 497–507.

Arán Carrión, J., Espín Estrella, A., Aznar Dols, F., Zamorano Toro, M., Rodríguez, M., & Ramos Ridao, A. (2008). Environmental decision-support systems for evaluating the carrying capacity of land areas: Optimal site selection for grid-connected photovoltaic power plants. *Renewable and Sustainable Energy Reviews*, *12*(9), 2358–2380. https://doi.org/10.1016/j.rser.2007.06.011

Armstrong, A., Ostle, N. J., & Whitaker, J. (2016). Solar park microclimate and vegetation management effects on grassland carbon cycling. *Environmental Research Letters*, *11*(7), 74016.

Barron-Gafford, G. A., Minor, R. L., Allen, N. A., Cronin, A. D., Brooks, A. E., & Pavao-Zuckerman, M. A. (2016). The Photovoltaic Heat Island Effect: Larger solar power plants increase local temperatures. *Scientific Reports*, *6*, srep35070. https://doi.org/10.1038/srep35070

Berens, P. (2009). CircStat: a MATLAB toolbox for circular statistics. *J Stat Softw*, *31*(10), 1–21.

Broxton, P. D., Zeng, X., Sulla-Menashe, D., & Troch, P. A. (2014). A global land cover climatology using MODIS data. *Journal of Applied Meteorology and Climatology*, *53*(6), 1593–1605.

Budyko, M. I. (Mikhail I. (1971). Climate and life. Retrieved from http://agris.fao.org/agris-search/search.do?recordID=US201300494263

Calaf, M., Parlange, M. B., & Meneveau, C. (2011). Large eddy simulation study of scalar transport in fully developed wind-turbine array boundary layers. *Physics of Fluids (1994-Present)*, *23*(12), 126603.

Charabi, Y., & Gastli, A. (2011). PV site suitability analysis using GIS-based spatial fuzzy multi-criteria evaluation. *Renewable Energy*, *36*(9), 2554–2561.

Chu, S., & Majumdar, A. (2012). Opportunities and challenges for a sustainable energy future. *Nature*, *488*(7411), 294.

Dai, K., Bergot, A., Liang, C., Xiang, W.-N., & Huang, Z. (2015). Environmental issues associated with wind energy – A review. *Renewable Energy*, *75*, 911–921. https://doi.org/10.1016/j.renene.2014.10.074

De Bruijn, S. L., & Bork, E. W. (2006). Biological control of Canada thistle in

temperate pastures using high density rotational cattle grazing. *Biological Control*, *36*(3), 305–315.

Dinesh, H., & Pearce, J. M. (2016). The potential of agrivoltaic systems. *Renewable and Sustainable Energy Reviews*, *54*, 299–308. https://doi.org/10.1016/j.rser.2015.10.024

Dupraz, C., Marrou, H., Talbot, G., Dufour, L., Nogier, A., & Ferard, Y. (2011a). Combining solar photovoltaic panels and food crops for optimising land use: Towards new agrivoltaic schemes. *Renewable Energy*, *36*(10), 2725–2732. https://doi.org/10.1016/j.renene.2011.03.005

Dupraz, C., Marrou, H., Talbot, G., Dufour, L., Nogier, A., & Ferard, Y. (2011b). Combining solar photovoltaic panels and food crops for optimising land use: Towards new agrivoltaic schemes. *Renewable Energy*, *36*(10), 2725–2732. https://doi.org/10.1016/j.renene.2011.03.005

Dupraz, C., Talbot, G., Marrou, H., Wery, J., Roux, S., Liagre, F., et al. (n.d.). To Mix or Not to Mix: Evidences for the Unexpected High Productivity of New Complex Agrivoltaic and Agroforestry Systems. 2011. *Available Onlin E: Https://Www. Researchgate. Net/Publication/230675951_To_ Mix_or_not_to_mix__evidences_for_the_unexpected_high_productivity_of_new_com plex_agrivoltaic_ And_agroforestry_systems (Accessed on 9 December 2015)*, 202–203.

Dupré, O., Vaillon, R., & Green, M. A. (2016). *Thermal behavior of photovoltaic devices: physics and engineering*. Springer.

EarthExplorer. (n.d.). Retrieved March 1, 2018, from https://earthexplorer.usgs.gov/

Hassanpour Adeh, E., Higgins, C. W., & Selker, J. S. (2017). Remarkable solar panels Influence on soil moisture, micrometeorology and water-use efficiency. Retrieved from https://ir.library.oregonstate.edu/xmlui/handle/1957/60846

Higgins, C. W., Vache, K., Calaf, M., Hassanpour, E., & Parlange, M. B. (2015). Wind turbines and water in irrigated areas. *Agricultural Water Management*, *152*, 299–300. https://doi.org/10.1016/j.agwat.2014.11.016

Hu, A., Levis, S., Meehl, G. A., Han, W., Washington, W. M., Oleson, K. W., et al. (2016). Impact of solar panels on global climate. *Nature Climate Change*, *6*(3), 290–

294. https://doi.org/10.1038/NCLIMATE2843

Huld, T., & Amillo, A. M. G. (2015). Estimating PV module performance over large geographical regions: The role of irradiance, air temperature, wind speed and solar spectrum. *Energies*, *8*(6), 5159–5181.

Kadowaki, M., Yano, A., Ishizu, F., Tanaka, T., & Noda, S. (2012). Effects of greenhouse photovoltaic array shading on Welsh onion growth. *Biosystems Engineering*, *111*(3), 290–297. https://doi.org/10.1016/j.biosystemseng.2011.12.006

Kratochvil, J. A., Boyson, W. E., & King, D. L. (2004). *Photovoltaic array performance model.* Sandia National Laboratories.

Krauter, S. (2004). Increased electrical yield via water flow over the front of photovoltaic panels. *Solar Energy Materials and Solar Cells*, *82*(1–2), 131–137.

Lewis, N. S., & Crabtree, G. (2005). *Basic research needs for solar energy utilization: report of the basic energy sciences workshop on solar energy utilization, April 18-21, 2005*. US Department of Energy, Office of Basic Energy Science.

Lewis, N. S., & Nocera, D. G. (2006). Powering the planet: Chemical challenges in solar energy utilization. *Proceedings of the National Academy of Sciences*, *103*(43), 15729–15735. https://doi.org/10.1073/pnas.0603395103

Li, X., Wagner, F., Peng, W., Yang, J., & Mauzerall, D. L. (2017). Reduction of solar photovoltaic resources due to air pollution in China. *Proceedings of the National Academy of Sciences*, *114*(45), 11867–11872. https://doi.org/10.1073/pnas.1711462114

Lin, C., Yang, K., Huang, J., Tang, W., Qin, J., Niu, X., et al. (2015). Impacts of wind stilling on solar radiation variability in China. *Scientific Reports*, *5*. https://doi.org/10.1038/srep15135

Marrou, H., Dufour, L., & Wery, J. (2013). How does a shelter of solar panels influence water flows in a soil–crop system? *European Journal of Agronomy*, *50*, 38–51. https://doi.org/10.1016/j.eja.2013.05.004

Marrou, H., Wéry, J., Dufour, L., & Dupraz, C. (2013). Productivity and radiation use efficiency of lettuces grown in the partial shade of photovoltaic panels. *European Journal of Agronomy*, *44*, 54–66.

Mellit, A., & Pavan, A. M. (2010). Performance prediction of 20kWp grid-connected

photovoltaic plant at Trieste (Italy) using artificial neural network. *Energy Conversion and Management*, *51*(12), 2431–2441. https://doi.org/10.1016/j.enconman.2010.05.007

Millstein, D., & Menon, S. (2011). Regional climate consequences of large-scale cool roof and photovoltaic array deployment. *Environmental Research Letters*, *6*(3), 34001.

Muradov, N. Z., & Veziroğlu, T. N. (2008). "Green" path from fossil-based to hydrogen economy: an overview of carbon-neutral technologies. *International Journal of Hydrogen Energy*, *33*(23), 6804–6839.

Nonhebel, S. (2005). Renewable energy and food supply: will there be enough land? *Renewable and Sustainable Energy Reviews*, *9*(2), 191–201.

Noorollahi, E., Fadai, D., Akbarpour Shirazi, M., & Ghodsipour, S. H. (2016). Land suitability analysis for solar farms exploitation using GIS and fuzzy analytic hierarchy process (FAHP)—a case study of Iran. *Energies*, *9*(8), 643.

Obama, B. (2017). The irreversible momentum of clean energy. *Science*, *355*(6321), 126–129. https://doi.org/10.1126/science.aam6284

On the temperature dependence of photovoltaic module electrical performance: A review of efficiency/power correlations - ScienceDirect. (n.d.). Retrieved August 17, 2017, from http://www.sciencedirect.com/science/article/pii/S0038092X08002788

Parkes, M. E., & Siam, N. (1979). Error associated with measurement of soil moisture change by neutron probe. *Journal of Agricultural Engineering Research*, *24*(1), 87–93.

Pavageau, M., & Schatzmann, M. (1999). Wind tunnel measurements of concentration fluctuations in an urban street canyon. *Atmospheric Environment*, *33*(24–25), 3961–3971.

Pookpunt, S., & Ongsakul, W. (2013). Optimal placement of wind turbines within wind farm using binary particle swarm optimization with time-varying acceleration coefficients. *Renewable Energy*, *55*, 266–276.

Porté-Agel, F., Wu, Y.-T., Lu, H., & Conzemius, R. J. (2011). Large-eddy simulation of atmospheric boundary layer flow through wind turbines and wind farms. *Journal of Wind Engineering and Industrial Aerodynamics*, *99*(4), 154–168.

PV-GIS: a web-based solar radiation database for the calculation of PV potential in Europe: International Journal of Sustainable Energy: Vol 24, No 2. (n.d.). Retrieved

December 26, 2017, from http://www.tandfonline.com/doi/abs/10.1080/14786450512331329556

R. Saidur, N. A. R. (2011). Environmental impact of wind energy. *Renewable and Sustainable Energy Reviews*, *15*(5), 2423–2430. https://doi.org/10.1016/j.rser.2011.02.024

Ramachandra, T. V., & Shruthi, B. V. (2007). Spatial mapping of renewable energy potential. *Renewable and Sustainable Energy Reviews*, *11*(7), 1460–1480. https://doi.org/10.1016/j.rser.2005.12.002

Ramli, M. A., Prasetyono, E., Wicaksana, R. W., Windarko, N. A., Sedraoui, K., & Al-Turki, Y. A. (2016). On the investigation of photovoltaic output power reduction due to dust accumulation and weather conditions. *Renewable Energy*, *99*, 836–844.

Ravi, S., Lobell, D. B., & Field, C. B. (2014). Tradeoffs and Synergies between Biofuel Production and Large Solar Infrastructure in Deserts. *Environmental Science & Technology*, *48*(5), 3021–3030. https://doi.org/10.1021/es404950n

Rodman, L. C., & Meentemeyer, R. K. (2006). A geographic analysis of wind turbine placement in Northern California. *Energy Policy*, *34*(15), 2137–2149.

Rogner, H. H., & others. (2012). *inGlobal Energy Assessment—Towards a Sustainable FutureCh. 7, 423–512*. Cambridge University Press.

Scherba, A., Sailor, D. J., Rosenstiel, T. N., & Wamser, C. C. (2011). Modeling impacts of roof reflectivity, integrated photovoltaic panels and green roof systems on sensible heat flux into the urban environment. *Building and Environment*, *46*(12), 2542–2551. https://doi.org/10.1016/j.buildenv.2011.06.012

Seidlova, L., Verlinden, M., Gloser, J., Milbau, A., & Nijs, I. (2009). Which plant traits promote growth in the low-light regimes of vegetation gaps? *Plant Ecology*, *200*(2), 303–318. https://doi.org/10.1007/s11258-008-9454-6

Shah, A., Torres, P., Tscharner, R., Wyrsch, N., & Keppner, H. (1999). Photovoltaic Technology: The Case for Thin-Film Solar Cells. *Science*, *285*(5428), 692–698. https://doi.org/10.1126/science.285.5428.692

Sheffield, J., Goteti, G., & Wood, E. F. (2006). c. *Journal of Climate*, *19*(13), 3088–3111. https://doi.org/10.1175/JCLI3790.1

Skoplaki, E., & Palyvos, J. A. (2009). On the temperature dependence of photovoltaic

module electrical performance: A review of efficiency/power correlations. *Solar Energy*, *83*(5), 614–624.

The Fowler Ridge Wind Farm Project, USA. (n.d.). Retrieved May 11, 2018, from https://www.power-technology.com/projects/fowlerridgewindfarmi/

Trancik, J. E. (2014). Renewable energy: Back the renewables boom. *Nature*, *507*(7492), 300–302. https://doi.org/10.1038/507300a

Turner, J. A. (1999). A Realizable Renewable Energy Future. *Science*, *285*(5428), 687–689. https://doi.org/10.1126/science.285.5428.687

Web Soil Survey - Home. (n.d.). Retrieved June 5, 2017, from https://websoilsurvey.sc.egov.usda.gov/App/HomePage.htm

Weiss, D. N. (2018). Predicted: Photovoltaic Plant Performance. *Joule*, *2*(2), 199–200. https://doi.org/10.1016/j.joule.2018.01.016

When will fossil fuel reserves be diminished? - ScienceDirect. (n.d.). Retrieved November 15, 2017, from http://www.sciencedirect.com/science/article/pii/S0301421508004126

W.M. Murphy, M. . J. (1976). *Grass varieties for central Oregon* (Agricultural Experiment Station Oregon State University, Corvallis No. Special Report 468).

Appendices

1.1 Appendix A: Average wind rose

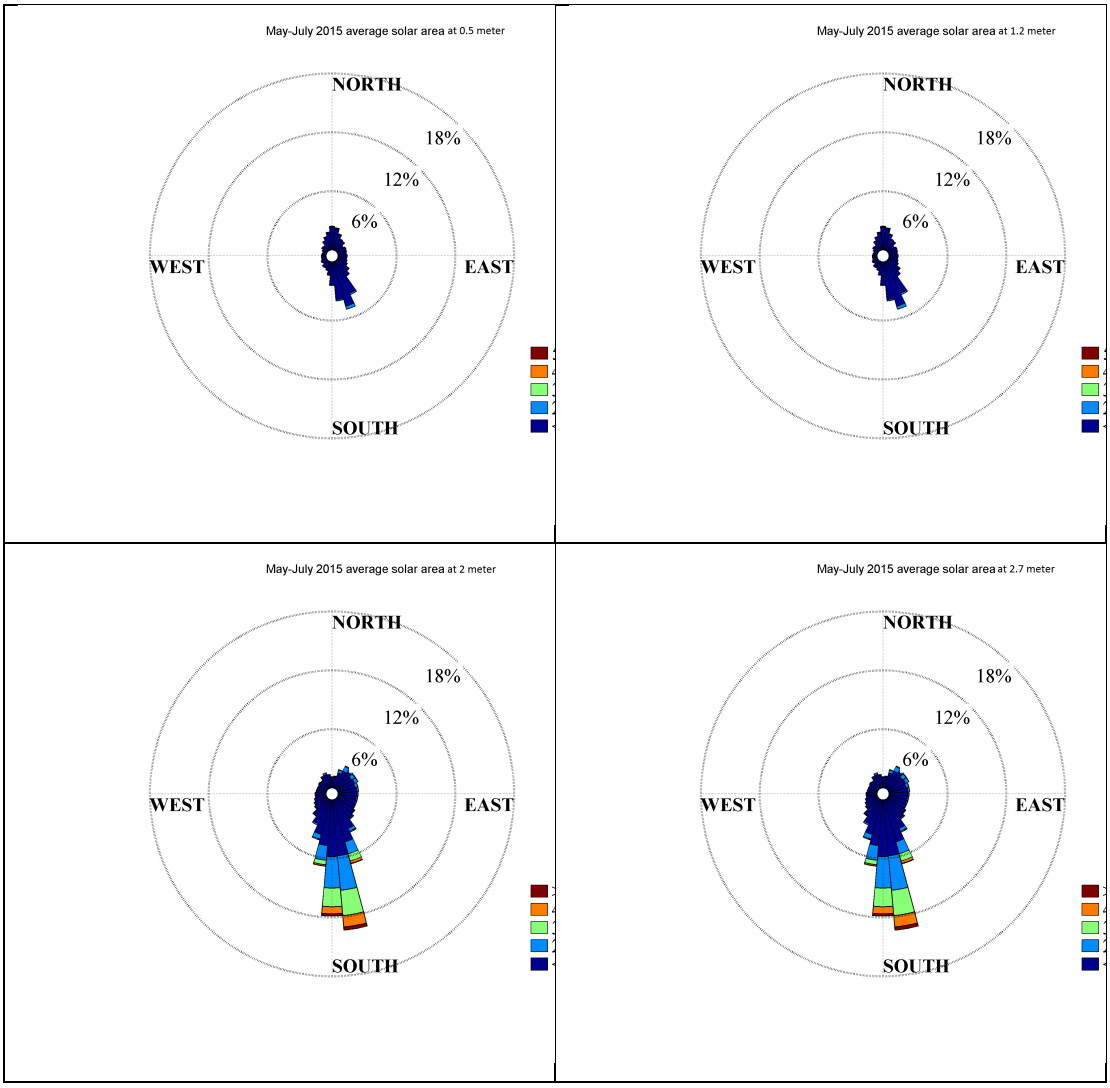

1.2 Appendix B: soil moisture profiles

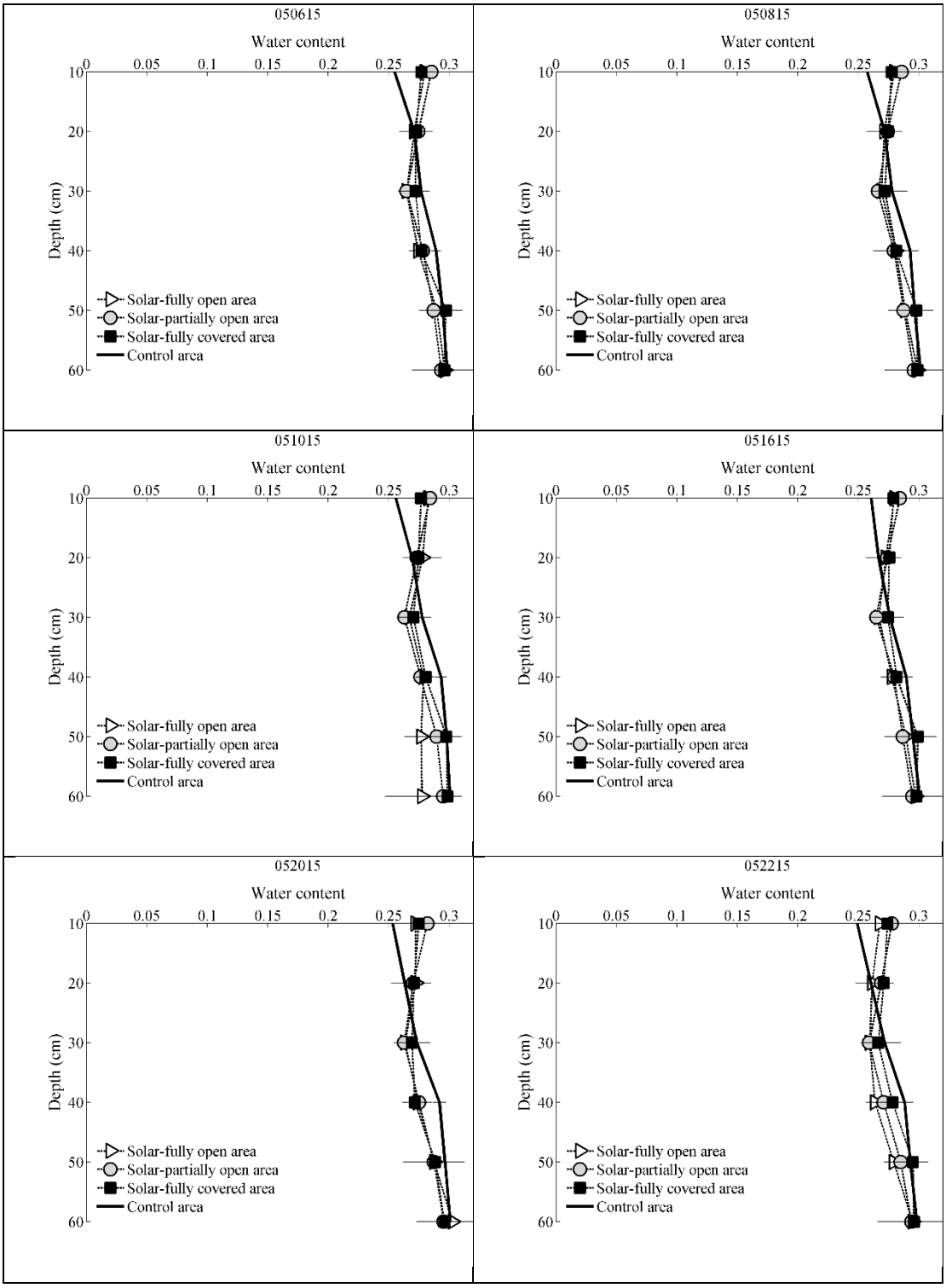

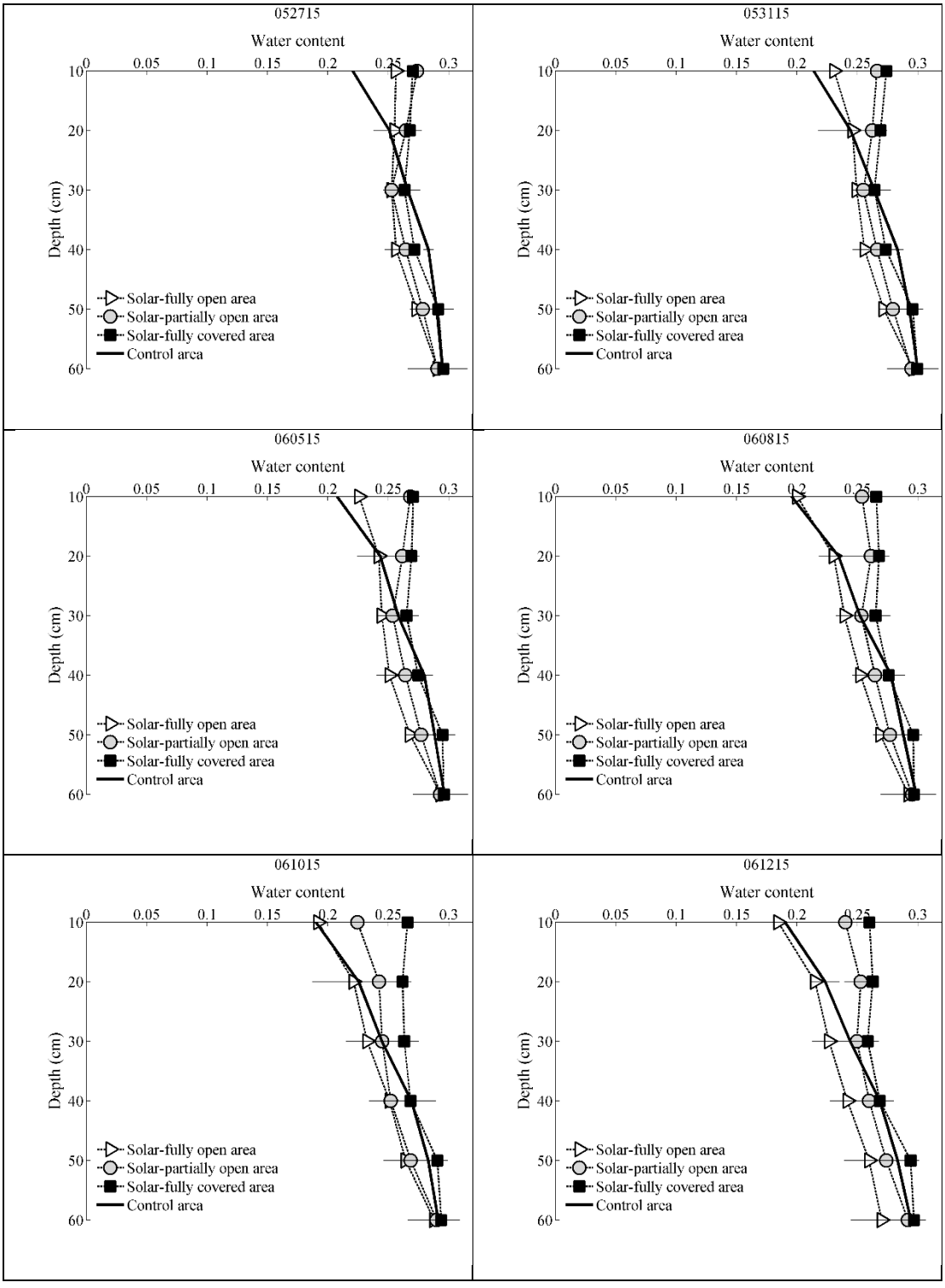
052715
053115
060515
060815
061015
061215
Water content
Depth (cm)
0
0.05
0.1
0.15
0.2
0.25
0.3
10
20
30
40
50
60
Solar-fully open area
Solar-partially open area
Solar-fully covered area
Control area

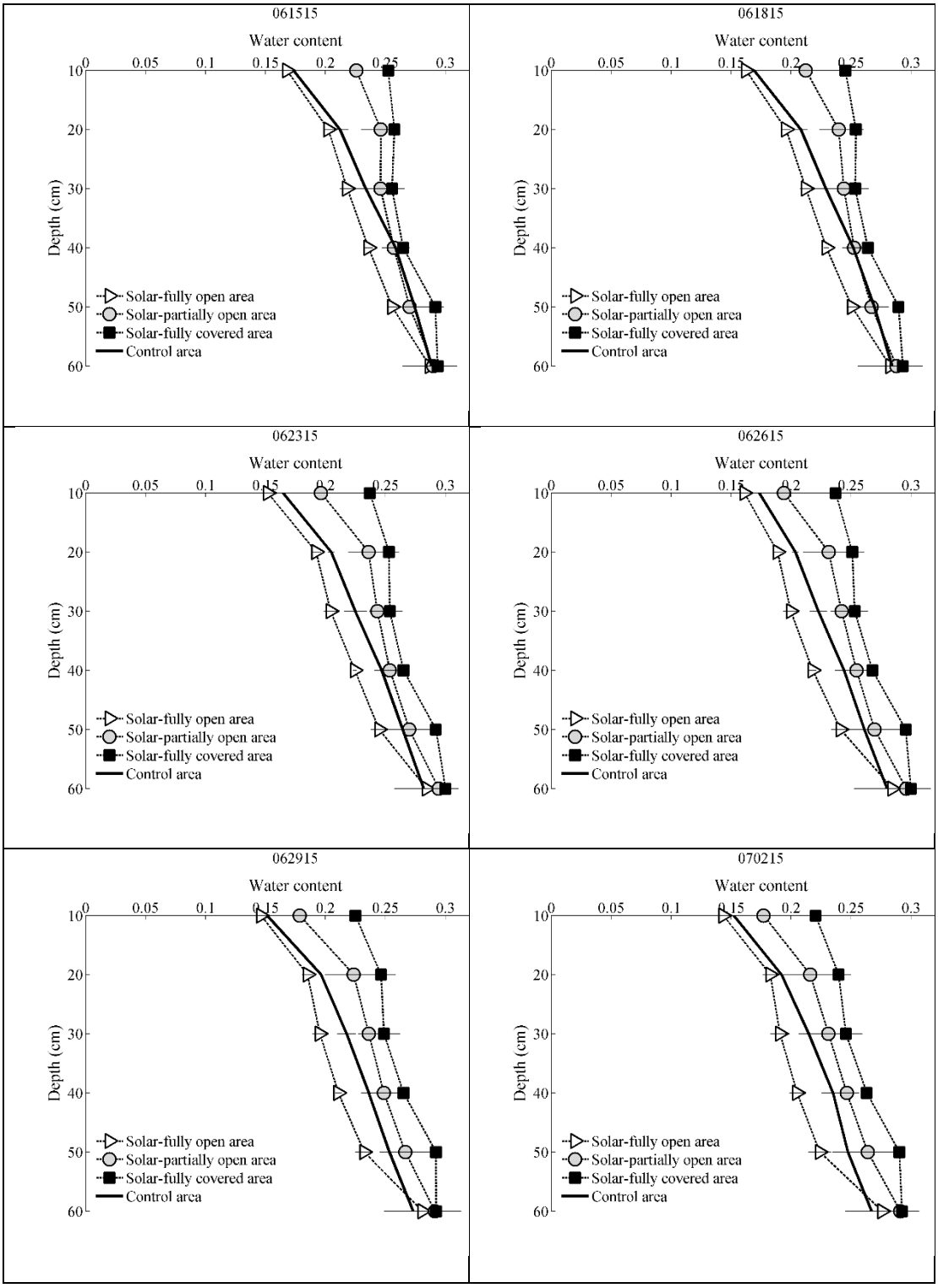
061515
Water content
0 0.05 0.1 0.15 0.2 0.25 0.3
10 20 30 40 50 60
Depth (cm)
Solar-fully open area
Solar-partially open area
Solar-fully covered area
Control area
061815
Water content
0 0.05 0.1 0.15 0.2 0.25 0.3
10 20 30 40 50 60
Depth (cm)
Solar-fully open area
Solar-partially open area
Solar-fully covered area
Control area
062315
Water content
0 0.05 0.1 0.15 0.2 0.25 0.3
10 20 30 40 50 60
Depth (cm)
Solar-fully open area
Solar-partially open area
Solar-fully covered area
Control area
062615
Water content
0 0.05 0.1 0.15 0.2 0.25 0.3
10 20 30 40 50 60
Depth (cm)
Solar-fully open area
Solar-partially open area
Solar-fully covered area
Control area
062915
Water content
0 0.05 0.1 0.15 0.2 0.25 0.3
10 20 30 40 50 60
Depth (cm)
Solar-fully open area
Solar-partially open area
Solar-fully covered area
Control area
070215
Water content
0 0.05 0.1 0.15 0.2 0.25 0.3
10 20 30 40 50 60
Depth (cm)
Solar-fully open area
Solar-partially open area
Solar-fully covered area
Control area

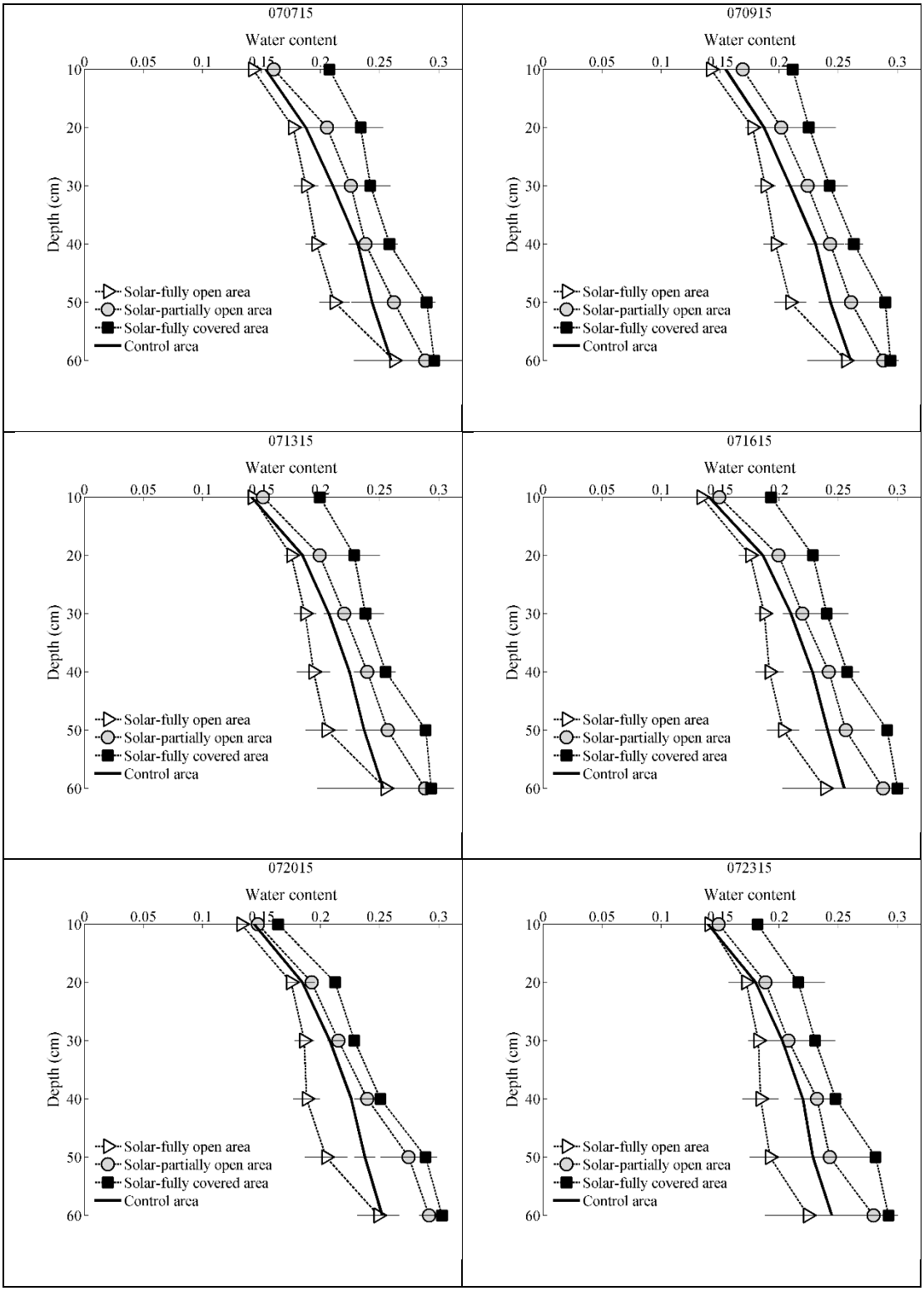
070715
Water content
0 0.05 0.1 0.15 0.2 0.25 0.3
10 20 30 40 50 60
Depth (cm)
Solar-fully open area
Solar-partially open area
Solar-fully covered area
Control area
070915
Water content
0 0.05 0.1 0.15 0.2 0.25 0.3
10 20 30 40 50 60
Depth (cm)
Solar-fully open area
Solar-partially open area
Solar-fully covered area
Control area
071315
Water content
0 0.05 0.1 0.15 0.2 0.25 0.3
10 20 30 40 50 60
Depth (cm)
Solar-fully open area
Solar-partially open area
Solar-fully covered area
Control area
071615
Water content
0 0.05 0.1 0.15 0.2 0.25 0.3
10 20 30 40 50 60
Depth (cm)
Solar-fully open area
Solar-partially open area
Solar-fully covered area
Control area
072015
Water content
0 0.05 0.1 0.15 0.2 0.25 0.3
10 20 30 40 50 60
Depth (cm)
Solar-fully open area
Solar-partially open area
Solar-fully covered area
Control area
072315
Water content
0 0.05 0.1 0.15 0.2 0.25 0.3
10 20 30 40 50 60
Depth (cm)
Solar-fully open area
Solar-partially open area
Solar-fully covered area
Control area

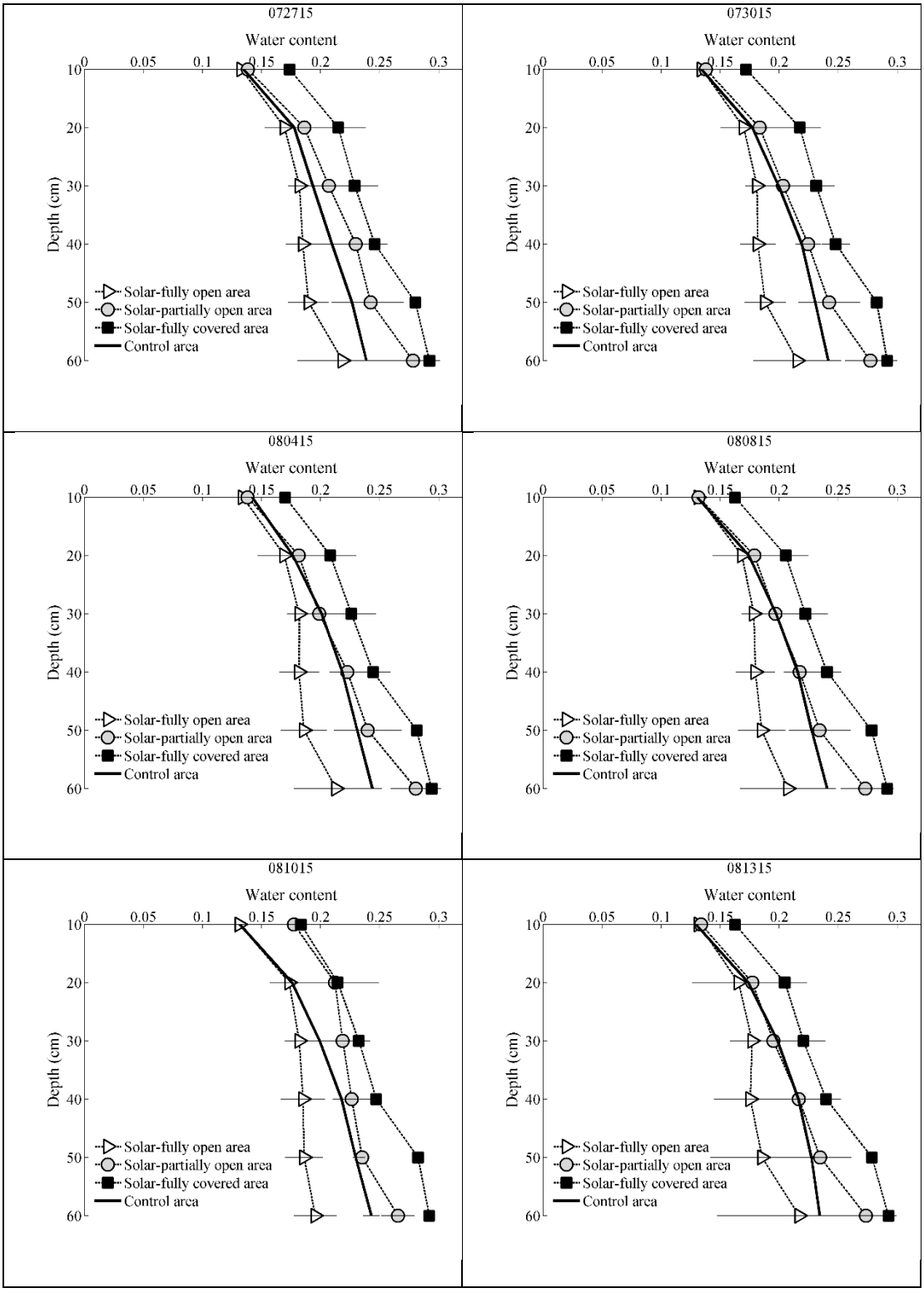
072715
073015
080415
080815
081015
081315
Water content
0 0.05 0.1 0.15 0.2 0.25 0.3
Depth (cm)
10 20 30 40 50 60
Solar-fully open area
Solar-partially open area
Solar-fully covered area
Control area

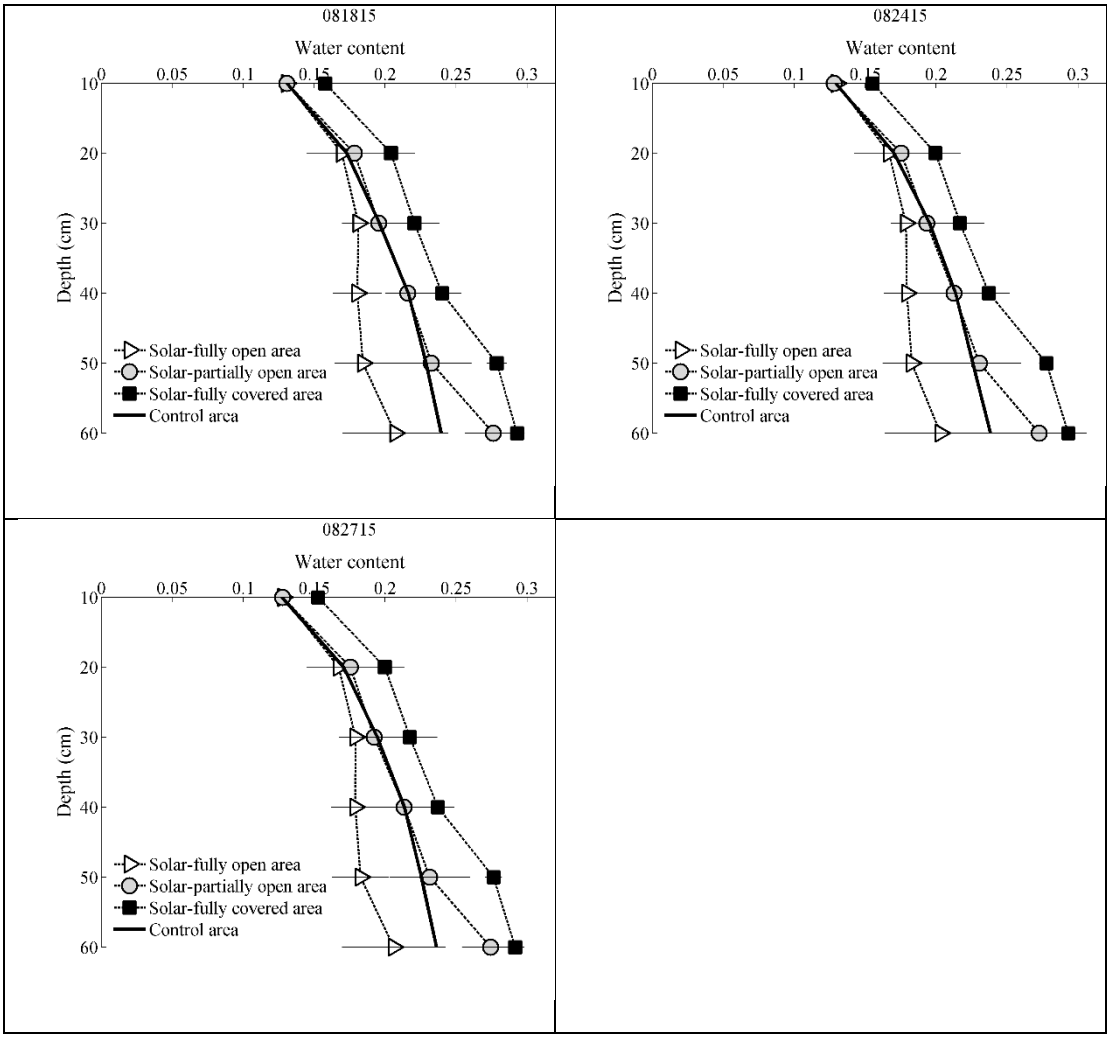
081815
Water content
0
0.05
0.1
0.15
0.2
0.25
0.3
10
20
30
40
50
60
Depth (cm)
Solar-fully open area
Solar-partially open area
Solar-fully covered area
Control area
082415
Water content
0
0.05
0.1
0.15
0.2
0.25
0.3
10
20
30
40
50
60
Depth (cm)
Solar-fully open area
Solar-partially open area
Solar-fully covered area
Control area
082715
Water content
0
0.05
0.1
0.15
0.2
0.25
0.3
10
20
30
40
50
60
Depth (cm)
Solar-fully open area
Solar-partially open area
Solar-fully covered area
Control area

1.3 Appendix C: water content time series

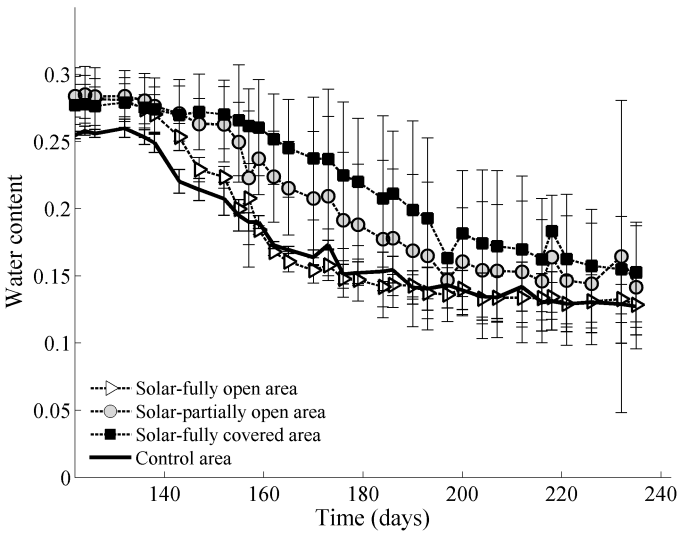

(a) 0.1 m

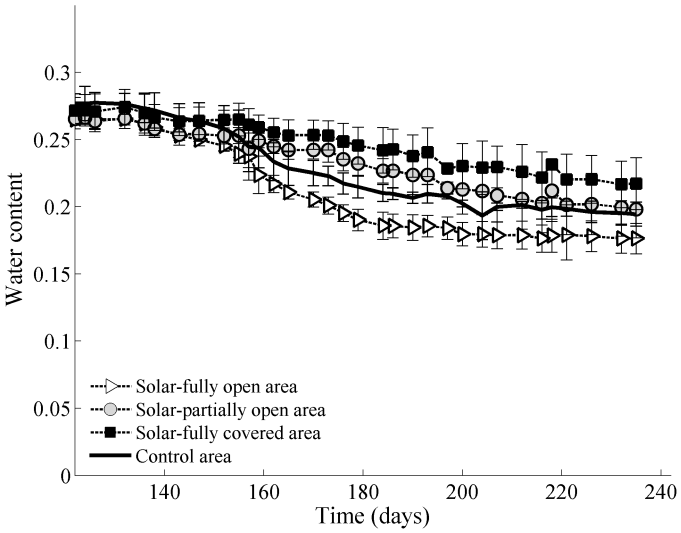

(b) 0.3 m

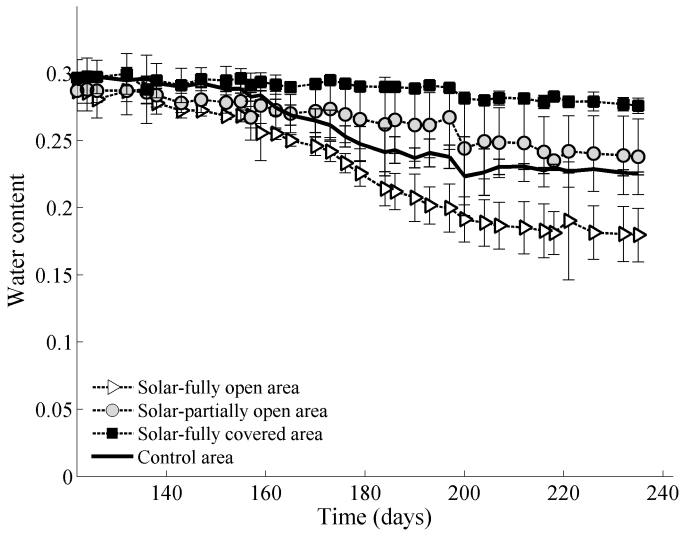
Water content
0.3
0.25
0.2
0.15
0.1
0.05
0
140
160
180
200
220
240
Time (days)
Solar-fully open area
Solar-partially open area
Solar-fully covered area
Control area

(c) 0.5 m